The Effective One Body description of the Two-Body problem

Thibault DAMOUR and Alessandro NAGAR

Institut des Hautes Études Scientifiques
35, route de Chartres
91440 – Bures-sur-Yvette (France)

Juin 2009

IHES/P/09/27

The Effective One Body description of the Two-Body problem

Thibault Damour and Alessandro Nagar

Abstract The Effective One Body (EOB) formalism is an analytical approach which aims at providing an accurate description of the motion and radiation of coalescing binary black holes with arbitrary mass ratio. We review the basic elements of this formalism and discuss its aptitude at providing accurate template waveforms to be used for gravitational wave data analysis purposes.

1 Introduction

A network of ground-based interferometric gravitational wave (GW) detectors (LIGO/VIRGO/GEO/...) is currently taking data near its planned sensitivity [1]. Coalescing black hole binaries are among the most promising, and most exciting, GW sources for these detectors. In order to successfully detect GWs from coalescing black hole binaries, and to be able to reliably measure the physical parameters of the source (masses, spins, ...), it is necessary to know in advance the shape of the GW signals emitted by inspiralling and merging black holes. Indeed, the detection and subsequent data analysis of GW signals is made by using a large bank of *templates* that accurately represent the GW waveforms emitted by the source.

Here, we shall introduce the reader to one promising strategy toward having an accurate analytical[1] description of the motion and radiation of binary black holes,

Thibault Damour
Institut des Hautes Etudes Scientifiques, 35 route de Chartres,
F-91440 Bures-sur-Yvette, France, e-mail: damour@ihes.fr

Alessandro Nagar
Institut des Hautes Etudes Scientifiques, 35 route de Chartres,
F-91440 Bures-sur-Yvette, France,
INFN, Sezione di Torino, Italy, e-mail: nagar@ihes.fr.

[1] Here we use the adjective "analytical" for methods that solve explicit (analytically given) ordinary differential equations (ODE), even if one uses standard (Runge-Kutta-type) numerical tools

which covers all its stages (inspiral, plunge, merger and ring-down): the *Effective One Body* approach [2, 3, 5, 4]. As early as 2000 [3] this method made several quantitative and qualitative predictions concerning the dynamics of the coalescence, and the corresponding GW radiation, notably: (i) a blurred transition from inspiral to a 'plunge' that is just a smooth continuation of the inspiral, (ii) a sharp transition, around the merger of the black holes, between a continued inspiral and a ring-down signal, and (iii) estimates of the radiated energy and of the spin of the final black hole. In addition, the effects of the individual spins of the black holes were investigated within the EOB [4, 6] and were shown to lead to a larger energy release for spins parallel to the orbital angular momentum, and to a dimensionless rotation parameter J/E^2 always smaller than unity at the end of the inspiral (so that a Kerr black hole can form right after the inspiral phase). All those predictions have been broadly confirmed by the results of the recent numerical simulations performed by several independent groups [7, 8, 9, 10, 11, 12, 13, 14, 15, 16, 17, 18, 19, 20, 21, 22, 23, 24, 25, 26, 27, 28, 29] (for a review of numerical relativity results see also [30]). Note that, in spite of the high computer power used in these simulations, the calculation of one sufficiently long waveform (corresponding to specific values of the many continuous parameters describing the two arbitrary masses, the initial spin vectors, and other initial data) takes on the order of two weeks. This is a very strong argument for developing analytical models of waveforms.

Those recent breakthroughs in numerical relativity (NR) open the possibility of comparing in detail the EOB description to NR results. This EOB/NR comparison has been initiated in several works [31, 32, 33, 34, 35, 36, 37, 38, 39, 40, 41]. The level of analytical/numerical agreement is unprecedented, compared to what has been previously achieved when comparing other types of analytical waveforms to numerical ones. In particular, Refs. [40, 41] have compared two different kind of analytical waveforms, computed within the EOB framework, to the most accurate gravitational waveform currently available from the Caltech-Cornell group, finding that the phase and amplitude differences are of the order of the numerical error.

If the reader wishes to put the EOB results in contrast with other (Post-Newtonian or hybrid) approaches he can consult, *e.g.*, [27, 28, 42, 43, 44, 45, 46, 47].

Before reviewing some of the technical aspects of the EOB method, let us indicate some of the historical roots of this method. First, we note that the EOB approach comprises three, rather separate, ingredients:

1. a description of the conservative (Hamiltonian) part of the dynamics of two black holes;
2. an expression for the radiation-reaction part of the dynamics;
3. a description of the GW waveform emitted by a coalescing binary system.

For each one of these ingredients, the essential inputs that are used in EOB works are high-order post-Newtonian (PN) expanded results which have been obtained by

to solve them. The important point is that, contrary to 3D numerical relativity simulations, numerically solving ODE's is extremely fast, and can therefore be done (possibly even in real time) for a dense sample of theoretical parameters, such as orbital ($\nu = m_1 m_2/M, \ldots$) or spin ($\hat{a}_1 = S_1/Gm_1^2, \theta_1, \varphi_1, \ldots$) parameters.

many years of work, by many researchers (see references below). However, one of the key ideas in the EOB philosophy is to avoid using PN results in their original "Taylor-expanded" form (*i.e.* $c_0 + c_1 v + c_2 v^2 + c_3 v^3 + \cdots + c_n v^n$), but to use them instead in some *resummed* form (*i.e.* some non-polynomial function of v, defined so as to incorporate some of the expected non-perturbative features of the exact result). The basic ideas and techniques for resumming each ingredient of the EOB are different and have different historical roots. Concerning the first ingredient, *i.e.* the EOB Hamiltonian, it was inspired by an approach to electromagnetically interacting quantum two-body systems introduced by Brézin, Itzykson and Zinn-Justin [48].

The resummation of the second ingredient, *i.e.* the EOB radiation-reaction force $\mathscr{F}$, was originally inspired by the Padé resummation of the flux function introduced by Damour, Iyer and Sathyaprakash [49]. Recently, a new and more sophisticated resummation technique for the radiation reaction force $\mathscr{F}$ has been introduced by Damour, Iyer and Nagar [50] and further employed in EOB/NR comparisons [40]. It will be discussed in detail below.

As for the third ingredient, *i.e.* the EOB description of the waveform emitted by a coalescing black hole binary, it was mainly inspired by the work of Davis, Ruffini and Tiomno [51] which discovered the transition between the plunge signal and a ringing tail when a particle falls into a black hole. Additional motivation for the EOB treatment of the transition from plunge to ring-down came from work on the, so-called, "close limit approximation" [52].

Let us finally note that the EOB approach has been recently improved [37, 50, 40] by following a methodology consisting of studying, element by element, the physics behind each feature of the waveform, and on systematically comparing various EOB-based waveforms with 'exact' waveforms obtained by NR approaches. Among these 'exact' NR waveforms, it has been useful to consider the small-mass-ratio limit [2] $\nu \equiv m_1 m_2/(m_1+m_2)^2 \ll 1$, in which one can use the well controllable 'laboratory' of numerical simulations of test particles (with an added radiation-reaction force) moving in black hole backgrounds [35, 36].

2 Motion and radiation of binary black holes: post-Newtonian expanded results

Before discussing the various resummation techniques used in the EOB approach, let us briefly recall the 'Taylor-expanded' results that have been obtained by pushing to high accuracies the post-Newtonian (PN) methods.

Concerning the orbital dynamics of compact binaries, we recall that the 2.5PN-accurate[3] equations of motion have been derived in the 1980's [53, 54, 55, 56].

[2] Beware that the fonts used in this chapter make the greek letter ν (indicating the symmetric mass ratio) look very similar to the latin letter $v \neq \nu$ indicating the velocity.

[3] As usual 'n-PN accuracy' means that a result has been derived up to (and including) terms which are $\sim (v/c)^{2n} \sim (GM/c^2 r)^n$ fractionally smaller than the leading contribution.

Pushing the accuracy of the equations of motion to the 3PN ($\sim (v/c)^6$) level proved to be a non-trivial task. At first, the representation of black holes by delta-function sources and the use of the (non diffeomorphism invariant) Hadamard regularization method led to ambiguities in the computation of the badly divergent integrals that enter the 3PN equations of motion [57, 58]. This problem was solved by using the (diffeomorphism invariant) *dimensional regularization* method (*i.e.* analytic continuation in the dimension of space d) which allowed one to complete the determination of the 3PN-level equations of motion [59, 60]. They have also been derived by an Einstein-Infeld-Hoffmann-type surface-integral approach [61]. The 3.5PN terms in the equations of motion are also known [62, 63, 64].

Concerning the emission of gravitational radiation, two different *gravitational-wave generation formalisms* have been developed up to a high PN accuracy: (i) the Blanchet-Damour-Iyer formalism [65, 66, 67, 68, 69, 70, 71] combines a multipolar post-Minkowskian (MPM) expansion in the exterior zone with a post-Newtonian expansion in the near zone; while (ii) the Will-Wiseman-Pati formalism [72, 73, 74, 62] uses a direct integration of the relaxed Einstein equations. These formalisms were used to compute increasingly accurate estimates of the gravitational waveforms emitted by inspiralling binaries. These estimates include both normal, near-zone generated post-Newtonian effects (at the 1PN [66], 2PN [75, 76, 72], and 3PN [77, 78] levels), and more subtle, wave-zone generated (linear and non-linear) 'tail effects' [69, 79, 80, 71]. However, technical problems arose at the 3PN level. Similarly to what happened with the equation of motion, the representation of black holes by 'delta-function' sources causes the appearance of dangerously divergent integrals in the 3PN multipole moments. The use of Hadamard (partie finie) regularization did not allow one to unambiguously compute the needed 3PN-accurate quadrupole moment. Only the use of the (formally) diffeomorphism-invariant *dimensional regularization* method allowed one to complete the 3PN-level gravitational-radiation formalism [82].

The works mentioned in this Section (see [83] for a detailed account and more references) finally lead to PN-expanded results for the motion and radiation of binary black holes. For instance, the 3.5PN equations of motion are given in the form ($a = 1,2$; $i = 1,2,3$)

$$\frac{d^2 z_a^i}{dt^2} = A_a^{i\,\mathrm{cons}} + A_a^{iRR}\,, \tag{1}$$

where

$$A^{\mathrm{cons}} = A_0 + c^{-2}A_2 + c^{-4}A_4 + c^{-6}A_6\,, \tag{2}$$

denotes the 'conservative' 3PN-accurate terms, while

$$A^{RR} = c^{-5}A_5 + c^{-7}A_7\,, \tag{3}$$

denotes the time-asymmetric contibutions, linked to 'radiation reaction'.

On the other hand, if we consider for simplicity the inspiralling motion of a quasi-circular binary system, the essential quantity describing the emitted gravitational waveform is the *phase* ϕ of the quadrupolar gravitational wave amplitude

$h(t) \simeq a(t)\cos(\phi(t)+\delta)$. PN theory allows one to derive several different functional expressions for the gravitational wave phase ϕ, as a function either of time or of the instantaneous frequency. For instance, as a function of time, ϕ admits the following explicit expansion in powers of $\theta \equiv \nu c^3(t_c - t)/5GM$ (where t_c denotes a formal 'time of coalescence', $M \equiv m_1 + m_2$ and $\nu \equiv m_1 m_2/M^2$)

$$\phi(t) = \phi_c - \nu^{-1}\,\theta^{5/8}\left(1 + \sum_{n=2}^{7}(a_n + a'_n \ln\theta)\,\theta^{-n/8}\right), \tag{4}$$

with some numerical coefficients a_n, a'_n which depend only on the dimensionless (symmetric) mass ratio $\nu \equiv m_1 m_2/M^2$. The derivation of the 3.5PN-accurate expansion (4) uses both the 3PN-accurate conservative acceleration (2) and a 3.5PN extension of the (fractionally) 1PN-accurate radiation reaction acceleration (3) obtained by assuming a balance between the energy of the binary system and the gravitational-wave energy flux at infinity (see, *e.g.*, [83]).

Among the many other possible ways [84] of using PN-expanded results to predict the GW phase $\phi(t)$, let us mention the semi-analytic T4 approximant [42, 32]. The GW phase defined by the T4 approximant happens to agree well during the inspiral with the NR phase in the equal mass case [27]. However, this agreement seems to be coincidental because the T4 phase exhibits significant disagreement with NR results for other mass ratios [39] (as well as for spinning black-holes [47]).

3 Conservative dynamics of binary black holes: the Effective One Body approach

The PN-expanded results briefly reviewed in the previous Section are expected to yield accurate descriptions of the motion and radiation of binary black holes only during their *early inspiralling* stage, *i.e.* as long as the PN expansion parameter $\gamma_e = GM/c^2R$ (where R is the distance between the two black holes) stays significantly smaller than the value $\sim \frac{1}{6}$ where the orbital motion is expected to become dynamically unstable ('last stable circular orbit' and beginning of a 'plunge' leading to the merger of the two black holes). One needs a better description of the motion and radiation to describe the *late inspiral* (say $\gamma_e \gtrsim \frac{1}{12}$), as well as the subsequent *plunge* and *merger*. One possible strategy for having a complete description of the motion and radiation of binary black holes, covering all the stages (inspiral, plunge, merger, ring-down), would then be to try to 'stitch together' PN-expanded analytical results describing the early inspiral phase with 3D numerical results describing the end of the inspiral, the plunge, the merger and the ring-down of the final black hole, see, *e.g.*, Refs. [86, 32].

However, we wish to argue that the EOB approach makes a better use of all the analytical information contained in the PN-expanded results (1)-(3). The basic claim (first made in [2, 3]) is that the use of suitable *resummation methods* should allow

one to describe, by analytical tools, a *sufficiently accurate* approximation of the *entire waveform*, from inspiral to ring-down, including the non-perturbative plunge and merger phases. To reach such a goal, one needs to make use of several tools: (i) resummation methods, (ii) exploitation of the flexibility of analytical approaches, (iii) extraction of the non-perturbative information contained in various numerical simulations, (iv) qualitative understanding of the basic physical features which determine the waveform.

Let us start by discussing the first tool used in the EOB approach: the systematic use of resummation methods. Essentially two resummation methods have been employed (and combined) and some evidence has been given that they do significantly improve the convergence properties of PN expansions. The first method is the systematic use of *Padé approximants*. It has been shown in Ref. [49] that near-diagonal Padé approximants of the radiation reaction force[4] $\mathscr{F}$ seemed to provide a good representation of $\mathscr{F}$ down to the last stable orbit (which is expected to occur when $R \sim 6GM/c^2$, *i.e.* when $\gamma_e \simeq \frac{1}{6}$). In addition, a new route to the resummation of $\mathscr{F}$ has been proposed very recently in Ref. [50]. This approach, that will be discussed in detail below, is based on a new multiplicative decomposition of the metric multipolar waveform (which is originally given as a standard PN series). In this case, Padé approximants prove to be useful to further improve the convergence properties of one particular factor of this multiplicative decomposition.

The second resummation method is a novel approach to the dynamics of compact binaries, which constitutes the core of the Effective One Body (EOB) method.

For simplicity of exposition, let us first explain the EOB method at the 2PN level. The starting point of the method is the 2PN-accurate Hamiltonian describing (in Arnowitt-Deser-Misner-type coordinates) the conservative, or time symmetric, part of the equations of motion (1) (*i.e.* the truncation $A^{\rm cons} = A_0 + c^{-2}A_2 + c^{-4}A_4$ of Eq. (2)) say $H_{\rm 2PN}(\boldsymbol{q}_1 - \boldsymbol{q}_2, \boldsymbol{p}_1, \boldsymbol{p}_2)$. By going to the center of mass of the system ($\boldsymbol{p}_1 + \boldsymbol{p}_2 = 0$), one obtains a PN-expanded Hamiltonian describing the *relative motion*, $\boldsymbol{q} = \boldsymbol{q}_1 - \boldsymbol{q}_2$, $\boldsymbol{p} = \boldsymbol{p}_1 = -\boldsymbol{p}_2$:

$$H^{\rm relative}_{\rm 2PN}(\boldsymbol{q},\boldsymbol{p}) = H_0(\boldsymbol{q},\boldsymbol{p}) + \frac{1}{c^2} H_2(\boldsymbol{q},\boldsymbol{p}) + \frac{1}{c^4} H_4(\boldsymbol{q},\boldsymbol{p}) \,, \tag{5}$$

where $H_0(\boldsymbol{q},\boldsymbol{p}) = \frac{1}{2\mu}\,\boldsymbol{p}^2 + \frac{GM\mu}{|\boldsymbol{q}|}$ (with $M \equiv m_1 + m_2$ and $\mu = m_1 m_2/M$) corresponds to the Newtonian approximation to the relative motion, while H_2 describes 1PN corrections and H_4 2PN ones. It is well known that, at the Newtonian approximation, $H_0(\boldsymbol{q},\boldsymbol{p})$ can be thought of as describing a 'test particle' of mass μ orbiting around an 'external mass' GM. The EOB approach is a *general relativistic generalization* of this fact. It consists in looking for an 'external spacetime geometry' $g^{\rm ext}_{\mu\nu}(x^\lambda; GM)$ such that the geodesic dynamics of a 'test particle' of mass μ within $g^{\rm ext}_{\mu\nu}(x^\lambda, GM)$ is

[4] We henceforth denote by $\mathscr{F}$ the *Hamiltonian* version of the radiation reaction term A^{RR}, Eq. (3), in the (PN-expanded) equations of motion. It can be heuristically computed up to (absolute) 5.5PN [77, 81, 82] and even 6PN [85] order by assuming that the energy radiated in gravitational waves at infinity is balanced by a loss of the dynamical energy of the binary system.

equivalent (when expanded in powers of $1/c^2$) to the original, relative PN-expanded dynamics (5).

Let us explain the idea, proposed in [2], for establishing a 'dictionary' between the real relative-motion dynamics, (5), and the dynamics of an 'effective' particle of mass μ moving in $g^{\rm ext}_{\mu\nu}(x^\lambda, GM)$. The idea consists in 'thinking quantum mechanically'[5]. Instead of thinking in terms of a classical Hamiltonian, $H(\boldsymbol{q},\boldsymbol{p})$ (such as $H^{\rm relative}_{\rm 2PN}$, Eq. (5)), and of its classical bound orbits, we can think in terms of the quantized energy levels $E(n,\ell)$ of the quantum bound states of the Hamiltonian operator $H(\hat{\boldsymbol{q}},\hat{\boldsymbol{p}})$. These energy levels will depend on two (integer valued) quantum numbers n and ℓ. Here (for a spherically symmetric interaction, as appropriate to $H^{\rm relative}$), ℓ parametrizes the total orbital angular momentum ($\boldsymbol{L}^2=\ell(\ell+1)\hbar^2$), while n represents the 'principal quantum number' $n=\ell+n_r+1$, where n_r (the 'radial quantum number') denotes the number of nodes in the radial wave function. The third 'magnetic quantum number' m (with $-\ell\leq m\leq\ell$) does not enter the energy levels because of the spherical symmetry of the two-body interaction (in the center of of mass frame). For instance, a non-relativistic Coulomb (or Newton!) interaction

$$H_0=\frac{1}{2\mu}\,\boldsymbol{p}^2+\frac{GM\mu}{|\boldsymbol{q}|} \tag{6}$$

gives rise to the well-known result

$$E_0(n,\ell)=-\frac{1}{2}\,\mu\left(\frac{GM\mu}{n\hbar}\right)^2, \tag{7}$$

which depends only on n (this is the famous Coulomb degeneracy). When considering the PN corrections to H_0, as in Eq. (5), one gets a more complicated expression of the form

$$E^{\rm relative}_{\rm 2PN}(n,\ell)=-\frac{1}{2}\mu\frac{\alpha^2}{n^2}\left[1+\frac{\alpha^2}{c^2}\left(\frac{c_{11}}{n\ell}+\frac{c_{20}}{n^2}\right)+\frac{\alpha^4}{c^4}\left(\frac{c_{13}}{n\ell^3}+\frac{c_{22}}{n^2\ell^2}+\frac{c_{31}}{n^3\ell}+\frac{c_{40}}{n^4}\right)\right], \tag{8}$$

where we have set $\alpha\equiv GM\mu/\hbar=Gm_1m_2/\hbar$, and where we consider, for simplicity, the (quasi-classical) limit where n and ℓ are large numbers. The 2PN-accurate result (8) had been derived by Damour and Schäfer [87] as early as 1988. The dimensionless coefficients c_{pq} are functions of the symmetric mass ratio $\nu\equiv\mu/M$, for instance $c_{40}=\frac{1}{8}(145-15\nu+\nu^2)$. In classical mechanics (*i.e.* for large n and ℓ), it is called the 'Delaunay Hamiltonian', *i.e.* the Hamiltonian expressed in terms of the *action variables*[6] $J=\ell\hbar=\frac{1}{2\pi}\oint p_\varphi\,d\varphi$, and $N=n\hbar=I_r+J$, with $I_r=\frac{1}{2\pi}\oint p_r\,dr$.

The energy levels (8) encode, in a gauge-invariant way, the 2PN-accurate relative dynamics of a 'real' binary. Let us now consider an auxiliary problem: the 'effective' dynamics of one body, of mass μ, following a geodesic in some 'external'

[5] This is related to an idea emphasized many times by John Archibald Wheeler: quantum mechanics can often help us in going to the essence of classical mechanics.

[6] We consider, for simplicity, 'equatorial' motions with $m=\ell$, *i.e.*, classically, $\theta=\frac{\pi}{2}$.

(spherically symmetric) metric[7]

$$g^{\rm ext}_{\mu\nu}\,dx^\mu\,dx^\nu = -A(R)\,c^2\,dT^2 + B(R)\,dR^2 + R^2(d\theta^2+\sin^2\theta\,d\varphi^2)\,. \tag{9}$$

Here, the *a priori unknown* metric functions $A(R)$ and $B(R)$ will be constructed in the form of expansions in GM/c^2R:

$$\begin{aligned} A(R) &= 1 + a_1\frac{GM}{c^2R} + a_2\left(\frac{GM}{c^2R}\right)^2 + a_3\left(\frac{GM}{c^2R}\right)^3 + \cdots\,;\\ B(R) &= 1 + b_1\frac{GM}{c^2R} + b_2\left(\frac{GM}{c^2R}\right)^2 + \cdots\,, \end{aligned} \tag{10}$$

where the dimensionless coefficients a_n, b_n depend on ν. From the Newtonian limit, it is clear that we should set $a_1 = -2$. By solving (by separation of variables) the 'effective' Hamilton-Jacobi equation

$$\begin{aligned} g^{\mu\nu}_{\rm eff}\,\frac{\partial S_{\rm eff}}{\partial x^\mu}\,\frac{\partial S_{\rm eff}}{\partial x^\nu} + \mu^2c^2 = 0\,,\\ S_{\rm eff} = -\mathscr{E}_{\rm eff}\,t + J_{\rm eff}\,\varphi + S_{\rm eff}(R)\,, \end{aligned} \tag{11}$$

one can straightforwardly compute (in the quasi-classical, large quantum numbers limit) the Delaunay Hamiltonian $\mathscr{E}_{\rm eff}(N_{\rm eff}, J_{\rm eff})$, with $N_{\rm eff} = n_{\rm eff}\,\hbar$, $J_{\rm eff} = \ell_{\rm eff}\,\hbar$ (where $N_{\rm eff} = J_{\rm eff} + I^{\rm eff}_R$, with $I^{\rm eff}_R = \frac{1}{2\pi}\oint p^{\rm eff}_R\,dR$, $P^{\rm eff}_R = \partial S_{\rm eff}(R)/dR$). This yields a result of the form

$$\begin{aligned} \mathscr{E}_{\rm eff}(n_{\rm eff},\ell_{\rm eff}) = \mu c^2 - \frac{1}{2}\,\mu\,\frac{\alpha^2}{n^2_{\rm eff}}\Bigg[1 + \frac{\alpha^2}{c^2}\left(\frac{c^{\rm eff}_{11}}{n_{\rm eff}\ell_{\rm eff}} + \frac{c^{\rm eff}_{20}}{n^2_{\rm eff}}\right)\\ + \frac{\alpha^4}{c^4}\left(\frac{c^{\rm eff}_{13}}{n_{\rm eff}\ell^3_{\rm eff}} + \frac{c^{\rm eff}_{22}}{n^2_{\rm eff}\ell^2_{\rm eff}} + \frac{c^{\rm eff}_{31}}{n^3_{\rm eff}\ell_{\rm eff}} + \frac{c^{\rm eff}_{40}}{n^4_{\rm eff}}\right)\Bigg], \end{aligned} \tag{12}$$

where the dimensionless coefficients $c^{\rm eff}_{pq}$ are now functions of the unknown coefficients a_n, b_n entering the looked for 'external' metric coefficients (10).

At this stage, one needs (as in the famous AdS/CFT correspondence) to define a 'dictionary' between the real (relative) two-body dynamics, summarized in Eq. (8), and the effective one-body one, summarized in Eq. (12). As, on both sides, quantum mechanics tells us that the action variables are quantized in integers ($N_{\rm real} = n\hbar$, $N_{\rm eff} = n_{\rm eff}\hbar$, etc.) it is most natural to identify $n = n_{\rm eff}$ and $\ell = \ell_{\rm eff}$. One then still needs a rule for relating the two different energies $E^{\rm relative}_{\rm real}$ and $\mathscr{E}_{\rm eff}$. Ref. [2] proposed to look for a general map between the real energy levels and the effective ones (which, as seen when comparing (8) and (12), cannot be directly identified because

[7] It is convenient to write the 'external metric' in Schwarzschild-like coordinates. Note that the external radial coordinate R differs from the two-body ADM-coordinate relative distance $R^{\rm ADM} = |\boldsymbol{q}|$. The transformation between the two coordinate systems has been determined in Refs. [2, 5].

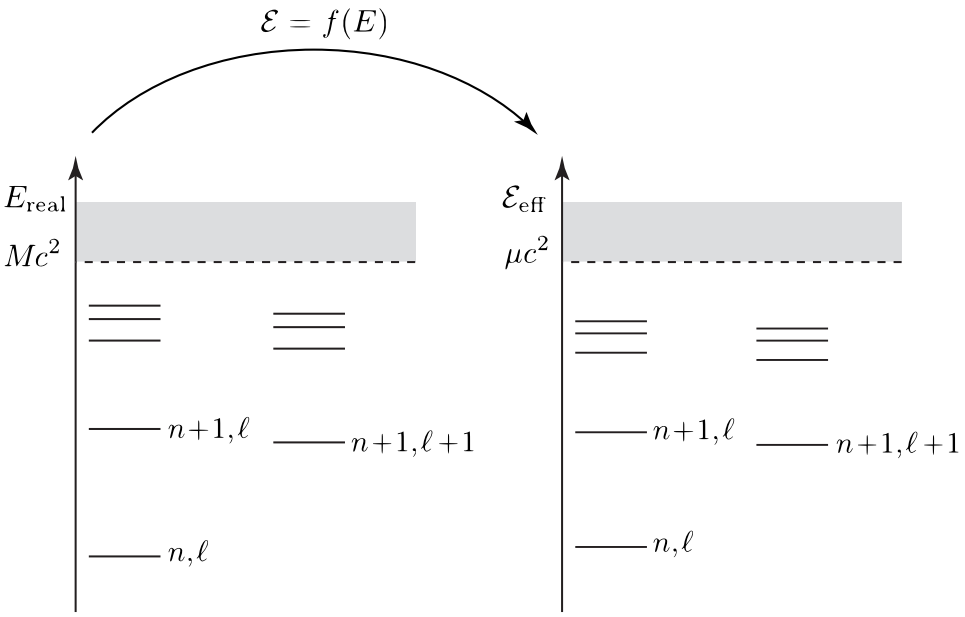

Fig. 1 Sketch of the correspondence between the quantized energy levels of the real and effective conservative dynamics. n denotes the 'principal quantum number' ($n = n_r + \ell + 1$, with $n_r = 0, 1, \ldots$ denoting the number of nodes in the radial function), while ℓ denotes the (relative) orbital angular momentum ($\boldsymbol{L}^2 = \ell(\ell+1)\hbar^2$). Though the EOB method is purely classical, it is conceptually useful to think in terms of the underlying (Bohr-Sommerfeld) quantization conditions of the action variables I_R and J to motivate the identification between n and ℓ in the two dynamics.

they do not include the same rest-mass contribution[8]), namely

$$\frac{\mathscr{E}_{\rm eff}}{\mu c^2} - 1 = f\left(\frac{E^{\rm relative}_{\rm real}}{\mu c^2}\right) = \frac{E^{\rm relative}_{\rm real}}{\mu c^2}\left(1 + \alpha_1 \frac{E^{\rm relative}_{\rm real}}{\mu c^2} + \alpha_2 \left(\frac{E^{\rm relative}_{\rm real}}{\mu c^2}\right)^2 + \cdots\right). \tag{13}$$

The 'correspondence' between the real and effective energy levels is illustrated in Fig. 1

Finally, identifying $\mathscr{E}_{\rm eff}(n,\ell)/\mu c^2$ to $f(E^{\rm relative}_{\rm real}/\mu c^2)$ yields six equations, relating the six coefficients $c^{\rm eff}_{pq}(a_2, a_3; b_1, b_2)$ to the six $c_{pq}(\nu)$ and to the two energy coefficients α_1 and α_2. It is natural to set $b_1 = +2$ (so that the linearized effective metric coincides with the linearized Schwarzschild metric with mass $M = m_1 + m_2$). One then finds that there exists a *unique* solution for the remaining five unknown coefficients a_2, a_3, b_2, α_1 and α_2. This solution is very simple:

$$a_2 = 0\,, \quad a_3 = 2\nu\,, \quad b_2 = 4 - 6\nu\,, \quad \alpha_1 = \frac{\nu}{2}\,, \quad \alpha_2 = 0\,. \tag{14}$$

[8] Indeed $E^{\rm total}_{\rm real} = Mc^2 + E^{\rm relative}_{\rm real} = Mc^2 + \text{Newtonian terms} + 1\text{PN}/c^2 + \cdots$, while $\mathscr{E}_{\rm effective} = \mu c^2 + N + 1\text{PN}/c^2 + \cdots$.

Note, in particular, that the map between the two energies is simply

$$\frac{\mathscr{E}_{\rm eff}}{\mu c^2} = 1 + \frac{E^{\rm relative}_{\rm real}}{\mu c^2}\left(1 + \frac{\nu}{2}\,\frac{E^{\rm relative}_{\rm real}}{\mu c^2}\right) = \frac{s - m_1^2 c^4 - m_2^2 c^4}{2\,m_1\,m_2\,c^4} \tag{15}$$

where $s = (\mathscr{E}^{\rm tot}_{\rm real})^2 \equiv (Mc^2 + E^{\rm relative}_{\rm real})^2$ is Mandelstam's invariant $= -(p_1 + p_2)^2$. Note also that, at 2PN accuracy, the crucial '$g^{\rm ext}_{00}$' metric coefficient $A(R)$ (which fully encodes the energetics of circular orbits) is given by the remarkably simple PN expansion

$$A_{\rm 2PN}(R) = 1 - 2u + 2\,\nu u^3\,, \tag{16}$$

where $u \equiv GM/(c^2 R)$ and $\nu \equiv \mu/M \equiv m_1 m_2/(m_1+m_2)^2$.

The dimensionless parameter $\nu \equiv \mu/M$ varies between 0 (in the test mass limit $m_1 \ll m_2$) and $\frac{1}{4}$ (in the equal-mass case $m_1 = m_2$). When $\nu \to 0$, Eq. (16) yields back, as expected, the well-known Schwarzschild time-time metric coefficient $-g^{\rm Schw}_{00} = 1 - 2u = 1 - 2GM/c^2 R$. One therefore sees in Eq. (16) the rôle of ν as a *deformation parameter* connecting a well-known test-mass result to a non trivial and new 2PN result. It is also to be noted that the 1PN EOB result $A_{\rm 1PN}(R) = 1 - 2u$ happens to be ν-independent, and therefore identical to $A^{\rm Schw} = 1 - 2u$. This is remarkable in view of the many non-trivial ν-dependent terms in the 1PN relative dynamics. The physically real 1PN ν-dependence happens to be fully encoded in the function $f(E)$ mapping the two energy spectra given in Eq. (15) above.

Let us emphasize the remarkable simplicity of the 2PN result (16). The 2PN Hamiltonian (5) contains eleven rather complicated ν-dependent terms. After transformation to the EOB format, the dynamical information contained in these eleven coefficients gets *condensed* into the very simple additional contribution $+2\,\nu u^3$ in $A(R)$, together with an equally simple contribution in the radial metric coefficient: $(A(R)\,B(R))_{\rm 2PN} = 1 - 6\,\nu u^2$. This condensation process is even more drastic when one goes to the next (conservative) post-Newtonian order: the 3PN level, i.e. additional terms of order $\mathscr{O}(1/c^6)$ in the Hamiltonian (5). As mentioned above, the complete obtention of the 3PN dynamics has represented quite a theoretical challenge and the final, resulting Hamiltonian is quite complicated. Even after going to the center of mass frame, the 3PN additional contribution $\frac{1}{c^6} H_6(\boldsymbol{q}, \boldsymbol{p})$ to Eq. (5) introduces eleven new complicated ν-dependent coefficients. After transformation to the EOB format [5], these eleven new coefficients get "condensed" into only *three* additional terms: (i) an additional contribution to $A(R)$, (ii) an additional contribution to $B(R)$, and (iii) a $\mathscr{O}(\boldsymbol{p}^4)$ modification of the 'external' geodesic Hamiltonian. For instance, the crucial 3PN $g^{\rm ext}_{00}$ metric coefficient becomes

$$A_{\rm 3PN}(R) = 1 - 2u + 2\,\nu u^3 + a_4\,\nu u^4\,, \tag{17}$$

where $u = GM/(c^2 R)$,

$$a_4 = \frac{94}{3} - \frac{41}{32}\,\pi^2 \simeq 18.6879027\,, \tag{18}$$

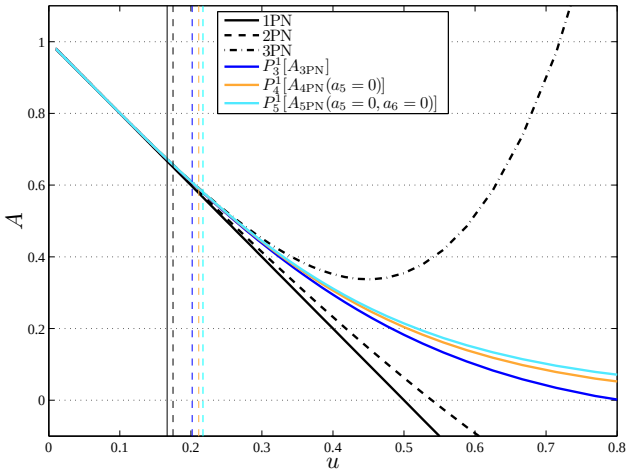

Fig. 2 Various approximations and Padé resummation of the EOB radial potential $A(u)$, where $u = GM/(c^2R)$, for the equal-mass case $\nu = 1/4$. The vertical dashed lines indicate the corresponding (adiabatic) LSO location [2] defined by the condition $d^2\hat{\mathscr{E}}^0_{\rm eff}/dR^2 = d\hat{\mathscr{E}}^0_{\rm eff}/dR = 0$, where $\hat{\mathscr{E}}^0_{\rm eff}$ is the effective energy along the sequence of circular orbits (*i.e.*, when $P_R^{\rm eff} = 0$).

while the additional contribution to $B(R)$ gives

$$D_{\rm 3PN}(R) \equiv (A(R)B(R))_{\rm 3PN} = 1 - 6\nu u^2 + 2(3\nu - 26)\nu u^3 \,. \tag{19}$$

Remarkably, it is found that the very simple 2PN energy map Eq. (15) does not need to be modified at the 3PN level.

The fact that the 3PN coefficient a_4 in the crucial 'effective radial potential' $A_{\rm 3PN}(R)$, Eq. (17), is rather large and positive indicates that the ν-dependent non-linear gravitational effects lead, for comparable masses ($\nu \sim \frac{1}{4}$), to a last stable (circular) orbit (LSO) which has a higher frequency and a larger binding energy than what a naive scaling from the test-particle limit ($\nu \to 0$) would suggest. Actually, the PN-expanded form (17) of $A_{\rm 3PN}(R)$ does not seem to be a good representation of the (unknown) exact function $A_{\rm EOB}(R)$ when the (Schwarzschild-like) relative coordinate R becomes smaller than about $6GM/c^2$ (which is the radius of the LSO in the test-mass limit). In fact, by continuity with the test-mass case, one a priori expects that $A_{\rm 3PN}(R)$ always exhibits a simple zero defining an EOB "effective horizon" that is smoothly connected to the Schwarzschild event horizon at $R = 2GM/c^2$ when $\nu \to 0$. However, the large value of the a_4 coefficient does actually prevent $A_{\rm 3PN}$ to have this property when ν is too large, and in particular when $\nu = 1/4$, as it is visually explained in Fig. 2. The black curves in the figure represent the A function at 1PN (solid line), 2PN (dashed line) and 3PN (dash-dot line) approximation: while the 2PN curve still has a simple zero, the 3PN does not, due to the large value

of a_4. It was therefore suggested [5] to further resum[9] $A_{3\rm PN}(R)$ by replacing it by a suitable Padé (P) approximant. For instance, the replacement of $A_{3\rm PN}(R)$ by

$$A^1_3(R) \equiv P^1_3[A_{3\rm PN}(R)] = \frac{1+n_1 u}{1+d_1 u + d_2 u^2 + d_3 u^3} \tag{20}$$

ensures that the $\nu = \frac{1}{4}$ case is smoothly connected with the $\nu = 0$ limit, as Fig. 2 clearly shows[10].

The use of Eq. (20) was suggested before one had any (reliable) non-perturbative information on the binding of close black hole binaries. Later, a comparison with some "waveless" numerical simulations of circular black hole binaries [89] has given some evidence that Eq. (20) is physically adequate. In Refs. [4, 89] it was also emphasized that, in principle, the comparison between numerical data and EOB-based predictions should allow one to determine the effect of the unknown higher PN contributions to Eq. (17). For instance, one can add a 4PN-like term $+a_5\nu u^5$ or a 5PN-like term $+a_6\nu u^6$ in Eq. (17), and then Padé the resulting radial function. The new *resummed A* potential will exhibit an explicit dependence on a_5 (at 4PN) or (a_5, a_6) (at 5PN), that is

$$A^1_4(R; a_5, \nu) = P^1_4\left[A_{3\rm PN}(R) + \nu a_5 u^5\right], \tag{21}$$

or

$$A^1_5(R; a_5, a_6, \nu) = P^1_5\left[A_{3\rm PN}(R) + \nu a_5 u^5 + \nu a_6 u^6\right]. \tag{22}$$

Comparing the predictions of $A^1_4(R; a_5, \nu)$ or $A^1_5(R; a_5, a_6, \nu)$ to numerical data might then determine what is the physically preferred "effective" value of the unknown coefficient a_5 (if working at 4PN effective accuracy) or of the doublet (a_5, a_6) (when including also 5PN corrections). For illustrative purposes, Fig. 2 shows the effect of the Padé resummation with $a_5 = a_6 = 0$ and $\nu = 1/4$. Note that the Padé resummation procedure is injecting some "information" beyond that contained in the numerical values of the PN expansion coefficients a_n's of $A(R)$. As a consequence, the operation of Padéing and of restricting a_5 and a_6 to the (3PN-compatible) values $a_5 = 0 = a_6$ do not commute: $A^1_4(R; 0, 1/4) \neq A^1_5(R; 0, 0, 1/4) \neq A^1_3(R, 1/4)$. In this respect, let us also mention that the 4PN a_5-dependent Padé approximant $A^1_4(R; a_5, \nu)$ exactly reduces to the 3PN Padé approximant $A^1_3(R; \nu)$ when a_5 is replaced by the following function of ν

$$a_5^{\rm 3PN}(\nu) \equiv \frac{\nu(3392 - 123\pi^2)^2}{18432(\nu - 4)}. \tag{23}$$

[9] The PN-expanded EOB building blocks $A(R), B(R), \ldots$ already represent a *resummation* of the PN dynamics in the sense that they have "condensed" the many terms of the original PN-expanded Hamiltonian within a very concise format. But one should not refrain to further resum the EOB building blocks themselves, if this is physically motivated.

[10] We recall that the coefficient n_1 and (d_1, d_2, d_3) of the Padé approximant are determined by the condition that the first four terms of the Taylor expansion of A^1_3 in powers of $u = GM/(c^2 R)$ coincide with $A_{3\rm PN}$.

Note that the value of the A_3^1-reproducing effective 4PN coefficient $a_5^{3\mathrm{PN}}(\nu)$ in the equal mass case is $a_5^{3\mathrm{PN}}(1/4) \simeq -17.158031$. This is numerically compatible with the value $a_5 = -17.16$ quoted in Ref. [28] (but note that the correct A_3^1-reproducing 4PN coefficient depends on the symmetric mass ratio ν). Similarly, when working at the 5PN level, $A_5^1(R;a_5,a_6,\nu)$ exactly reduces to the 4PN Padé approximant $A_4^1(R;a_5,\nu)$ when a_6 is replaced by the following function of both ν and a_5:

$$a_6^{4\mathrm{PN}}(\nu,a_5) \equiv \frac{\nu\left(2304a_5^2+96\left(3392-123\pi^2\right)a_5+\left(3776-123\pi^2\right)\left(32(3\nu+94)-123\pi^2\right)\right)}{24\left[\left(3776-123\pi^2\right)\nu-1536\right]}. \tag{24}$$

The use of numerical relativity data to constrain the values of the higher PN parameters (a_5,a_6) is an example of the useful *flexibility* [88] of analytical approaches: the fact that one can tap numerically-based, non-perturbative information to improve the EOB approach. The flexibility of the EOB approach related to the use of the a_5-dependent radial potential $A_4^1(R;a_5,\nu)$ has been exploited in several recent works [33, 37, 38, 39, 28, 41] focusing on the comparison of EOB-based waveforms with waveforms computed via numerical relativity simulations. Collectively, all these studies have shown that it is possible to constrain a_5 (together with other flexibility parameters related to the resummation of radiation reaction, see below) so as to yield an excellent agreement (at the level of the published numerical errors) between EOB and numerical relativity waveforms. The result, however, cannot be summarized by stating that a_5 is constrained to be in the vicinity of a special numerical value. Rather, one finds a strong correlation between a_5 and other parameters, notably the radiation reaction parameter v_{pole} introduced below. More recently, Ref. [40] could get rid of the flexibility parameters (such as v_{pole}) related to the resummation of radiation reaction, and has shown that one can get an excellent agreement with numerical relativity data by using *only* the flexibility in the doublet (a_5,a_6) (the other parameters being essentially fixed internally to the formalism). We shall discuss this result further in Sec. 5 below.

The same kind of ν-continuity argument discussed so far for the A function needs to be applied also to the $D(R)_{3\mathrm{PN}}$ function defined in Eq. (19). A straightforward way to ensure that the D function stays positive when R decreases (since it is $D=1$ when $\nu \to 0$) is to replace $D_{3\mathrm{PN}}(R)$ by $D_3^0(R) \equiv P_3^0\left[D_{3\mathrm{PN}}(R)\right]$, where P_3^0 indicates the $(0,3)$ Padé approximant and explicitly reads

$$D_3^0(R) = \frac{1}{1+6\nu u^2-2(3\nu-26)\nu u^3}. \tag{25}$$

The resummation of A (via Padé approximants) is necessary for ensuring the existence and ν-continuity of a *last stable orbit* (see vertical lines in Fig. 2), as well as the existence and ν-continuity of a *last unstable orbit*, i.e. of a ν-deformed analog of the light ring $R = 3GM/c^2$ when $\nu \to 0$. We recall that, when $\nu = 0$, the light ring corresponds to the circular orbit of a massless particle, or of an extremely rel-

ativistic massive particle, and is technically defined by looking for the maximum of $A(R)/R^2$, i.e. by solving $(d/dR)(A(R)/R^2)=0$. When $\nu\neq 0$ and when considering the quasi-circular plunge following the crossing of the last stable orbit, the "effective" meaning of the "ν-deformed light ring" (technically defined by solving $(d/dR)(A(R:\nu)/R^2)=0$) is to entail, in its vicinity, the existence of a maximum of the orbital frequency $\Omega = d\varphi/dt$ (the resummation of $D(R)$ plays a useful role in ensuring the ν-continuity of this plunge behavior).

4 Description of radiation-reaction effects in the Effective One Body approach

In the previous Section we have described how the EOB method encodes the conservative part of the relative orbital dynamics into the dynamics of an 'effective' particle. Let us now briefly discuss how to complete the EOB dynamics by defining some *resummed* expressions describing radiation reaction effects. One is interested in circularized binaries, which have lost their initial eccentricity under the influence of radiation reaction. For such systems, it is enough (as shown in [3]) to include a radiation reaction force in the p_φ equation of motion only. More precisely, we are using phase space variables $r, p_r, \varphi, p_\varphi$ associated to polar coordinates (in the equatorial plane $\theta=\frac{\pi}{2}$). Actually it is convenient to replace the radial momentum p_r by the momentum conjugate to the 'tortoise' radial coordinate $R_*=\int dR(B/A)^{1/2}$, *i.e.* $P_{R_*}=(A/B)^{1/2}P_R$. The real EOB Hamiltonian is obtained by first solving Eq. (15) to get $E^{\rm total}_{\rm real}=\sqrt{s}$ in terms of $\mathscr{E}_{\rm eff}$, and then by solving the effective Hamiltonian-Jacobi equation[11] to get $\mathscr{E}_{\rm eff}$ in terms of the effective phase space coordinates $\boldsymbol{q}_{\rm eff}$ and $\boldsymbol{p}_{\rm eff}$. The result is given by two nested square roots (we henceforth set $c=1$):

$$\hat{H}_{\rm EOB}(r,p_{r_*},\varphi)=\frac{H^{\rm real}_{\rm EOB}}{\mu}=\frac{1}{\nu}\sqrt{1+2\nu\,(\hat{H}_{\rm eff}-1)}\,, \tag{26}$$

where

$$\hat{H}_{\rm eff}=\sqrt{p^2_{r_*}+A(r)\left(1+\frac{p^2_\varphi}{r^2}+z_3\,\frac{p^4_{r_*}}{r^2}\right)}\,, \tag{27}$$

with $z_3=2\nu\,(4-3\nu)$. Here, we are using suitably rescaled dimensionless (effective) variables: $r=R/GM$, $p_{r_*}=P_{R_*}/\mu$, $p_\varphi=P_\varphi/\mu\,GM$, as well as a rescaled time $t=T/GM$. This leads to equations of motion $(r,\varphi,p_{r_*},p_\varphi)$ of the form

[11] Completed by the $\mathscr{O}(\boldsymbol{p}^4)$ terms that must be introduced at 3PN.

$$\frac{d\varphi}{dt} = \frac{\partial \hat{H}_{\rm EOB}}{\partial p_\varphi} \equiv \Omega \,, \tag{28}$$

$$\frac{dr}{dt} = \left(\frac{A}{B}\right)^{1/2} \frac{\partial \hat{H}_{\rm EOB}}{\partial p_{r_*}} \,, \tag{29}$$

$$\frac{dp_\varphi}{dt} = \hat{\mathscr{F}}_\varphi \,, \tag{30}$$

$$\frac{dp_{r_*}}{dt} = -\left(\frac{A}{B}\right)^{1/2} \frac{\partial \hat{H}_{\rm EOB}}{\partial r} \,, \tag{31}$$

which explicitly read

$$\frac{d\varphi}{dt} = \frac{A p_\varphi}{\nu r^2 \hat{H} \hat{H}_{\rm eff}} \equiv \Omega \,, \tag{32}$$

$$\frac{dr}{dt} = \left(\frac{A}{B}\right)^{1/2} \frac{1}{\nu \hat{H} \hat{H}_{\rm eff}} \left(p_{r_*} + z_3 \frac{2A}{r^2} p_{r_*}^3 \right) \,, \tag{33}$$

$$\frac{dp_\varphi}{dt} = \hat{\mathscr{F}}_\varphi \,, \tag{34}$$

$$\frac{dp_{r_*}}{dt} = -\left(\frac{A}{B}\right)^{1/2} \frac{1}{2\nu \hat{H} \hat{H}_{\rm eff}} \left\{ A' + \frac{p_\varphi^2}{r^2} \left(A' - \frac{2A}{r} \right) + z_3 \left(\frac{A'}{r^2} - \frac{2A}{r^3} \right) p_{r_*}^4 \right\} \,, \tag{35}$$

where $A' = dA/dr$. As explained above the EOB metric function $A(r)$ is defined by Padé resumming the Taylor-expanded result (10) obtained from the matching between the real and effective energy levels (as we were mentioning, one uses a similar Padé resumming for $D(r) \equiv A(r)B(r)$). One similarly needs to resum $\hat{\mathscr{F}}_\varphi$, i.e., the φ component of the radiation reaction which has been introduced on the r.h.s. of Eq. (30). During the quasi-circular inspiral $\hat{\mathscr{F}}_\varphi$ is known (from the PN work mentioned in Section 2 above) in the form of a Taylor expansion of the form

$$\hat{\mathscr{F}}_\varphi^{\rm Taylor} = -\frac{32}{5} \nu \Omega^5 r_\omega^4 \hat{F}^{\rm Taylor}(v_\varphi) \,, \tag{36}$$

where $v_\varphi \equiv \Omega r_\omega$, and $r_\omega \equiv r[\psi(r,p_\varphi)]^{1/3}$ is a modified EOB radius, with ψ being defined as

$$\psi(r,p_\varphi) = \frac{2}{r^2} \left(\frac{dA(r)}{dr} \right)^{-1} \left[1 + 2\nu \left(\sqrt{A(r) \left(1 + \frac{p_\varphi^2}{r^2} \right)} - 1 \right) \right] , \tag{37}$$

which generalizes the 2PN-accurate Eq. (22) of Ref. [90]. In Eq. (36) we have defined

$$\begin{aligned} \hat{F}^{\rm Taylor}(v) = 1 &+ A_2(\nu) v^2 + A_3(\nu) v^3 + A_4(\nu) v^4 + A_5(\nu) v^5 \\ &+ A_6(\nu, \log v) v^6 + A_7(\nu) v^7 + A_8(\nu = 0, \log v) v^8 \,, \end{aligned} \tag{38}$$

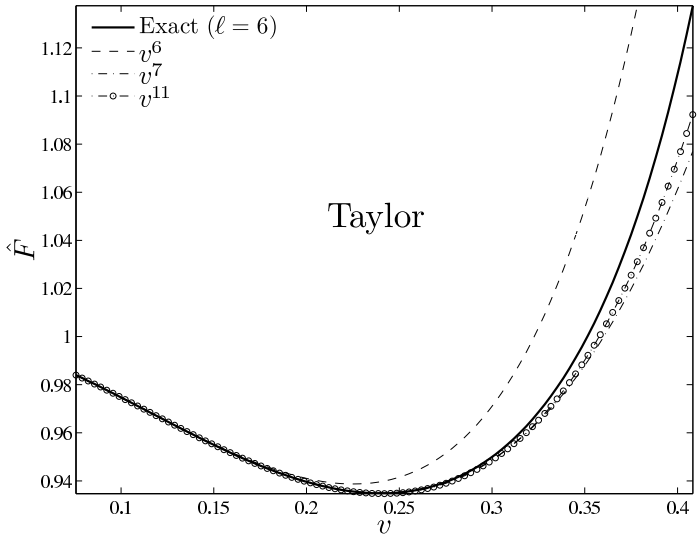

Fig. 3 The extreme-mass-ratio limit ($\nu = 0$): the Newton-normalized energy flux emitted by a particle on circular orbits. The figure illustrates the scattering of the standard Taylor expansion of the flux around the "exact" numerical result (computed up to $\ell = 6$) obtained via perturbation theory.

where we have added to the known 3.5PN-accurate comparable-mass result the small-mass-ratio 4PN contribution [91]. We recall that the small-mass contribution to the Newton-normalized flux is actually known up to 5.5PN order, i.e. to v^{11} included. The standard Taylor expansion of the flux, (38), has rather poor convergence properties when considered up to the LSO. This is illustrated in Fig. 3 in the small-mass limit $\nu = 0$. The convergence of the PN-expanded flux can be studied in detail in the $\nu = 0$ limit, because in this case one can compute an "exact" result numerically (using black hole perturbation theory [92, 93]). The "exact" energy flux shown in Fig. 3 is obtained as a sum over multipoles

$$F^{\ell max} = \sum_{\ell=2}^{\ell_{\rm max}} \sum_{m=1}^{\ell} F_{\ell m}, \tag{39}$$

where $F_{\ell m} = F_{\ell |m|}$ already denotes the sum of two equal contributions corresponding to $+m$ and $-m$ ($m \neq 0$ as $F_{\ell 0}$ vanishes for circular orbits). To be precise, the "exact" result exhibited in Fig. 3 is given by the rather accurate approximation $F^{(6)}$ obtained by choosing $\ell_{\rm max} = 6$; i.e., by truncating the sum over ℓ in Eq. (39) beyond $\ell = 6$. In addition, one normalizes the result onto the "Newtonian" (i.e., quadrupolar) result $F_{22}^N = 32/5(\mu/M)^2 v^{10}$. In other words, the solid line in Fig. 3 represents the quantity $\hat{F} \equiv F^{(6)}/F_{22}^N$.

For clarity, we selected only three Taylor approximants: 3PN (v^6), 3.5PN (v^7) and 5.5PN (v^{11}). These three values suffice to illustrate the rather large scatter

among Taylor approximants, and the fact that, near the LSO, the convergence towards the exact value (solid line) is rather slow, and non monotonic. [See also Fig. 1 in Ref. [94] and Fig. 3 of Ref. [49] for fuller illustrations of the scattered and non monotonic way in which successive Taylor expansions approach the numerical result.] The results shown in Fig. 3 elucidate that the Taylor series (38) is inadequate to give a reliable representation of the energy loss during the plunge. That is the reason why the EOB formalism advocates the use of a "resummed" version of $\mathscr{F}_\varphi$, i.e. a nonpolynomial function replacing Eq. (38) at the r.h.s. of the Hamilton's equation (and coinciding with it in in the $v/c \ll 1$ limit).

Two methods have been proposed to perform such a resummation. The first method, that strongly relies on the use of Padé approximants, was introduced by Damour, Iyer and Sathyaprakash [49] and, with different degrees of sophistication, has been widely used in the literature dealing with the EOB formalism [3, 6, 31, 35, 32, 33, 34, 36, 37, 38, 39, 28, 41]. The second resummation method has been recently introduced by Damour, Iyer and Nagar [50] and exploited to provide a self-consistent expression of the radiation reaction force in Ref. [40]. This latter resummation procedure is based on (i) a new multiplicative decomposition of the gravitational metric waveform which yields a (ii) resummation of each multipolar contribution to the energy flux. The use of Padé approximants is a useful tool (but not the only one) that proves helpful to further improve the convergence properties of each multipolar contribution to the flux. The following two Sections are devoted to highlighting the main features of the two methods. For pedagogical reasons the calculation is first done in the small-mass limit ($\nu \to 0$) and then generalized to the comparable mass case.

4.1 Resummation of $\hat{F}^{\rm Taylor}$ using a one-parameter family of Padé approximants: tuning $v_{\rm pole}$

Following [49], one resums $\hat{F}^{\rm Taylor}$ by using the following Padé resummation approach. First, one chooses a certain number $v_{\rm pole}$ which is intended to represent the value of the orbital velocity v_φ at which the exact angular momentum flux would become infinite if one were to formally analytically continue $\hat{\mathscr{F}}_\varphi$ along *unstable* circular orbits below the Last Stable Orbit (LSO): then, given $v_{\rm pole}$, one defines the resummed $\hat{F}(v_\varphi)$ as

$$\hat{F}^{\rm resummed}(v_\varphi) = \left(1 - \frac{v_\varphi}{v_{\rm pole}}\right)^{-1} P_4^4 \left[\left(1 - \frac{v_\varphi}{v_{\rm pole}}\right) \hat{F}^{\rm Taylor}(v_\varphi; \nu = 0)\right], \qquad (40)$$

where P_4^4 denotes a $(4,4)$ Padé approximant.

If one first follows the reasoning line of [49], and fixes the location of the pole in the resummed flux at the standard Schwarzschild value $v_{\rm pole}^{(\nu=0)} = 1/\sqrt{3}$, one gets the result in Fig. 4. By comparison to Fig. 3, one can appreciate the significantly better

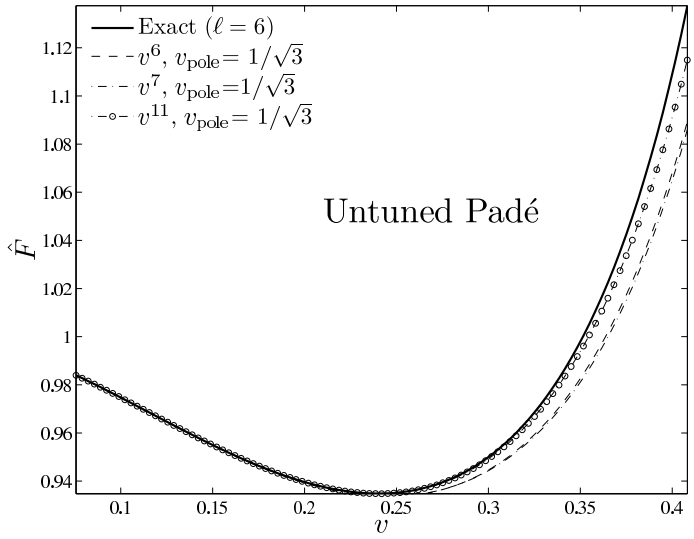

Fig. 4 The extreme-mass-ratio limit ($\nu = 0$). Padé resummation of the Taylor expandend energy flux of Fig. 3 as proposed in Ref. [49] with $v_{\rm pole} = 1/\sqrt{3}$. The sequence of Padé approximants is less scattered than the corresponding Taylor ones and closer to the exact result.

(and monotonic) way in which successive *Padé approximants* approach (in L_∞ norm on the full interval $0 < x < x_{\rm LSO}$) the numerical result. Ref. [49] also showed that the observationally relevant overlaps (of both the "faithfulness" and the "effectualness" types) between analytical and numerical adiabatic signals were systematically better for Padé approximants than for Taylor ones. Note that this figure is slightly different from the corresponding results in panel *(b)* of Fig. 3 in [49] (in particular, the present result exhibits a better "convergence" of the v^{11} curve). This difference is due to the new treatment of the logarithmic terms $\propto \log x$. Instead of factoring them out in front as proposed in [49], we consider them here (following [37]) as being part of the "Taylor coefficients" $f_n(\log x)$ when Padéing the flux function.

A remarkable improvement in the (L_∞) closeness between $\hat{F}^{\text{Padé-resummed}}(v)$ and $\hat{F}^{\rm Exact}(v)$ can be obtained, as suggested by Damour and Nagar [37] (following ideas originally introduced in Ref. [97]), by suitably flexing the value of $v_{\rm pole}$. As proposed in Ref. [37], $v_{\rm pole}$ is tuned until the difference between the resummed and the exact flux at the LSO is zero (or at least smaller than 10^{-4}). The resulting closeness between the exact and tuned-resummed fluxes is illustrated in Fig. 5. It is so good (compared to the previous figures, where the differences were clearly visible) that we need to complement the figure with Table 1. This table compares in a quantitative way the result of the "untuned" Padé resummation ($v_{\rm pole} = 1/\sqrt{3}$) of Ref. [49] to the result of the "$v_{\rm pole}$-tuned" Padé resummation described here. Defining the function $\Delta\hat{F}(v; v_{\rm pole}) = \hat{F}^{\rm Resummed}(v; v_{\rm pole}) - \hat{F}^{\rm Exact}(v)$ measuring the difference between a resummed and the exact energy flux, Table 1 lists both the values of $\Delta\hat{F}$ at $v = v_{\rm LSO}$ and its L_∞ norm on the interval $0 < v < v_{\rm LSO}$ for both the untuned and tuned cases.

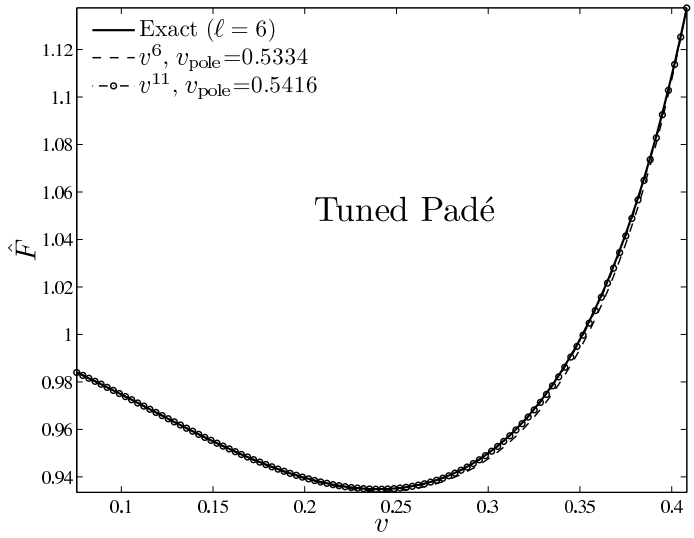

Fig. 5 The extreme mass ratio limit ($\nu = 0$). Same of Fig. 4 but *flexing* the value of the parameter $v_{\rm pole}$ so to improve the agreement with the exact result.

Table 1 Errors in the flux of the two (untuned or tuned) Padé resummation procedures. From left to right, the columns report: the PN-order; the difference between the resummed and the exact flux, $\Delta\hat{F} = \hat{F}^{\rm Resummed} - \hat{F}^{\rm Exact}$, at the LSO, and the L_∞ norm of $\Delta\hat{F}$, $||\Delta\hat{F}||_\infty$ (computed over the interval $0 < v < v_{\rm LSO}$), for $v_{\rm pole} = 1/\sqrt{3}$; the *flexed* value of $v_{\rm pole}$ used here; $\Delta\hat{F}$ at the LSO and the corresponding L_∞ norm (over the same interval) for the flexed value of $v_{\rm pole}$.

PN-order	$\Delta\hat{F}^{1/\sqrt{3}}_{\rm LSO}$	$\|\|\Delta\hat{F}\|\|^{1/\sqrt{3}}_\infty$	$v_{\rm pole}$	$\Delta\hat{F}^{v_{\rm pole}}_{\rm LSO}$	$\|\|\Delta\hat{F}\|\|^{v_{\rm pole}}_\infty$
3 (v^6)	-0.048	0.048	0.5334	7.06×10^{-5}	0.00426
3.5 (v^7)	-0.051	0.051	0.5425	5.50×10^{-5}	0.00429
5.5 (v^{11})	-0.022	0.022	0.5416	2.52×10^{-5}	0.000854

Note, in particular, how the $v_{\rm pole}$-flexing approach permits to reduce the L_∞ norm over this interval by more than an order of magnitude with respect to the untuned case. Note that the closeness between the tuned flux and the exact one is remarkably good (4.3×10^{-3}) already at the 3PN level.

It has recently been shown in several works [37, 38, 39, 41] that the *flexibility* in the choice of $v_{\rm pole}$ could be advantageously used to get a close agreement with NR data (at the level of the numerical error). We will not comment here any further on this *parameter-dependent* resummation procedure of the energy flux and address the reader to the aforementioned references for further details.

4.2 Parameter-free resummation of waveform and energy flux

In this section we shall introduce the reader to the new resummation technique for the multipolar waveform (and thus for the energy flux) introduced in Ref. [36, 37] and perfected in [50]. The aim is to summarize here the main ideas discussed in [50] as well as to collect most of the relevant equations that are useful for implementation in the EOB dynamics. To be precise, the new results discussed in Ref. [50] are twofold: on the one hand, that work generalized the $\ell = m = 2$ resummed waveform of [36, 37] to higher multipoles by using the most accurate currently known PN-expanded results [99, 100, 101] as well as the higher PN terms which are known in the test-mass limit [95, 96]; on the other hand, it introduced a *new resummation procedure* which consists in considering a new theoretical quantity, denoted as $\rho_{\ell m}(x)$, which enters the (ℓ,m) waveform (together with other building blocks, see below) only through its ℓ-th power: $h_{\ell m} \propto (\rho_{\ell m}(x))^{\ell}$. Here, and below, x denotes the invariant PN-ordering parameter $x \equiv (GM\Omega/c^3)^{2/3}$.

The main novelty introduced by Ref. [50] is to write the (ℓ,m) multipolar waveform emitted by a circular nonspinning compact binary as the *product* of several factors, namely

$$h^{(\varepsilon)}_{\ell m} = \frac{GM\nu}{c^2 R} n^{(\varepsilon)}_{\ell m} c_{\ell+\varepsilon}(\nu) x^{(\ell+\varepsilon)/2} Y^{\ell-\varepsilon,-m}\left(\frac{\pi}{2}, \Phi\right) \hat{S}^{(\varepsilon)}_{\rm eff} T_{\ell m} e^{{\rm i}\delta_{\ell m}} \rho^{\ell}_{\ell m}. \qquad (41)$$

Here ε denotes the parity of $\ell+m$ ($\varepsilon = \pi(\ell+m)$), i.e. $\varepsilon = 0$ for "even-parity" (mass-generated) multipoles ($\ell+m$ even), and $\varepsilon = 1$ for "odd-parity" (current-generated) ones ($\ell+m$ odd); $n^{(\varepsilon)}_{\ell m}$ and $c_{\ell+\varepsilon}(\nu)$ are numerical coefficients; $\hat{S}^{(\varepsilon)}_{\rm eff}$ is a μ-normalized effective source (whose definition comes from the EOB formalism); $T_{\ell m}$ is a resummed version [36, 37] of an infinite number of "leading logarithms" entering the *tail effects* [69, 103]; $\delta_{\ell m}$ is a supplementary phase (which corrects the phase effects not included in the *complex* tail factor $T_{\ell m}$), and, finally, $(\rho_{\ell m})^{\ell}$ denotes the ℓ-th power of the quantity $\rho_{\ell m}$ which is the new building block introduced in [50]. Note that in previous papers [36, 37] the quantity $(\rho_{\ell m})^{\ell}$ was denoted as $f_{\ell m}$ and we will mainly use this notation below. Before introducing explicitly the various elements entering the waveform (41) it is convenient to decompose $h_{\ell m}$ as

$$h_{\ell m} = h^{(N,\varepsilon)}_{\ell m} \hat{h}^{(\varepsilon)}_{\ell m}, \qquad (42)$$

where $h^{(N,\varepsilon)}_{\ell m}$ is the Newtonian contribution and $\hat{h}^{(\varepsilon)}_{\ell m} \equiv \hat{S}^{(\varepsilon)}_{\rm eff} T_{\ell m} e^{{\rm i}\delta_{\ell m}} f_{\ell m}$ represents a resummed version of all the PN corrections. The PN correcting factor $\hat{h}^{(\varepsilon)}_{\ell m}$, as well as all its building blocks, has the structure $\hat{h^{(\varepsilon)}}_{\ell m} = 1 + \mathcal{O}(x)$.

Entering now in the discussion of the explicit form of the elements entering Eq. (41), we have that the ν-independent numerical coefficients are given by

$$n^{(0)}_{\ell m} = (\mathrm{i}m)^\ell \frac{8\pi}{(2\ell+1)!!}\sqrt{\frac{(\ell+1)(\ell+2)}{\ell(\ell-1)}}, \tag{43}$$

$$n^{(1)}_{\ell m} = -(\mathrm{i}m)^\ell \frac{16\pi\mathrm{i}}{(2\ell+1)!!}\sqrt{\frac{(2\ell+1)(\ell+2)(\ell^2-m^2)}{(2\ell-1)(\ell+1)\ell(\ell-1)}}, \tag{44}$$

while the ν-dependent coefficients $c_{\ell+\varepsilon}(\nu)$ (such that $|c_{\ell+\varepsilon}(\nu=0)|=1$), can be expressed in terms of ν (as in Ref. [99, 101]), although they are more conveniently written in terms of the two mass ratios $X_1 = m_1/M$ and $X_2 = m_2/M$ in the form

$$\begin{aligned} c_{\ell+\varepsilon}(\nu) &= X_2^{\ell+\varepsilon-1} + (-)^{\ell+\varepsilon} X_1^{\ell+\varepsilon-1} \\ &= X_2^{\ell+\varepsilon-1} + (-)^m X_1^{\ell+\varepsilon-1}. \end{aligned} \tag{45}$$

In the second form of the equation we have used the fact that, as $\varepsilon = \pi(\ell+m)$, $\pi(\ell+\varepsilon) = \pi(m)$.

Let us turn now to discussing the structure of the $\hat{S}^{(\varepsilon)}_{\rm eff}$ and $T_{\ell m}$ factors. To this aim, following Ref. [50], we recall that the along the sequence of EOB circular orbits, which are determined by the condition $\partial_u \left\{A(u)[1+j_0^2 u^2]\right\} = 0$, the effective EOB Hamiltonian (per unit μ mass) reads

$$\hat{H}_{\rm eff} = \frac{H_{\rm eff}}{\mu} = \sqrt{A(u)(1+j_0^2 u^2)} \quad \text{(circular orbits)}. \tag{46}$$

where the squared angular momentum is given by

$$j_0^2(u) = -\frac{A'(u)}{(u^2 A(u))'} \quad \text{(circular orbits)}, \tag{47}$$

with the prime denoting d/du. Inserting this u-parametric representation of j^2 in Eq. (46) defines the u-parametric representation of the effective Hamiltonian $\hat{H}_{\rm eff}(u)$. In the even-parity case (corresponding to mass moments), since the leading order source of gravitational radiation is given by the energy density, Ref. [50] defined the even-parity "source factor" as

$$\hat{S}^{(0)}_{\rm eff}(x) = \hat{H}_{\rm eff}(x) \qquad \ell+m \quad \text{even}, \tag{48}$$

where $x = (GM\Omega/c^3)^{2/3}$. In the odd-parity case, they explored two, equally motivated, possibilities. The first one consists simply in still factoring $\hat{H}_{\rm eff}(x)$; i.e., in defining $\hat{S}^{(1,H)}_{\rm eff} = \hat{H}_{\rm eff}(x)$ also when $\ell+m$ is odd. The second one consists in factoring the angular momentum $\mathscr{J}$. Indeed, the angular momentum density $\varepsilon_{ijk}x^j\tau^{0k}$ enters as a factor in the (odd-parity) current moments, and $\mathscr{J}$ occurs (in the small-ν limit) as a factor in the source of the Regge-Wheeler-Zerilli odd-parity multipoles. This leads us to define as second possibility

$$\hat{S}^{(1,J)}_{\rm eff} = \hat{j}(x) \equiv x^{1/2} j(x) \qquad \ell+m \quad \text{odd}, \tag{49}$$

where $\hat{j}$ denotes what can be called the "Newton-normalized" angular momentum, namely the ratio $\hat{j}(x) = j(x)/j_N(x)$ with $j_N(x) = 1/\sqrt{x}$. In Ref. [50] the relative merits of the two possible choices were discussed. Although the analysis in the adiabatic $\nu = 0$ limit showed that they are equivalent from the practical point of view (because they both yield waveforms that are very close to the exact numerical result) we prefer to consider only the J-factorization in the following, that we will treat as our standard choice.

The second building block in our factorized decomposition is the "tail factor" $T_{\ell m}$ (introduced in Refs. [36, 37]). As mentioned above, $T_{\ell m}$ is a resummed version of an infinite number of "leading logarithms" entering the transfer function between the near-zone multipolar wave and the far-zone one, due to *tail effects* linked to its propagation in a Schwarzschild background of mass $M_{\rm ADM} = H^{\rm real}_{\rm EOB}$. Its explicit expression reads

$$T_{\ell m} = \frac{\Gamma(\ell+1-2{\rm i}\hat{\hat{k}})}{\Gamma(\ell+1)} e^{\pi\hat{\hat{k}}} e^{2{\rm i}\hat{\hat{k}}\log(2kr_0)}, \tag{50}$$

where $r_0 = 2GM$ and $\hat{\hat{k}} \equiv GH^{\rm real}_{\rm EOB} m\Omega$ and $k \equiv m\Omega$. Note that $\hat{\hat{k}}$ differs from k by a rescaling involving the *real* (rather than the *effective*) EOB Hamiltonian, computed at this stage along the sequence of circular orbits.

The tail factor $T_{\ell m}$ is a complex number which already takes into account some of the dephasing of the partial waves as they propagate out from the near zone to infinity. However, as the tail factor only takes into account the leading logarithms, one needs to correct it by a complementary dephasing term, $e^{{\rm i}\delta_{\ell m}}$, linked to subleading logarithms and other effects. This subleading phase correction can be computed as being the phase $\delta_{\ell m}$ of the complex ratio between the PN-expanded $\hat{h}^{(\varepsilon)}_{\ell m}$ and the above defined source and tail factors. In the comparable-mass case ($\nu \neq 0$), the 3PN δ_{22} phase correction to the leading quadrupolar wave was originally computed in Ref. [37] (see also Ref. [36] for the $\nu = 0$ limit). Full results for the subleading partial waves to the highest possible PN-accuracy by starting from the currently known 3PN-accurate ν-dependent waveform [101] have been obtained in [50].

The last factor in the multiplicative decomposition of the multipolar waveform can be computed as being the modulus $f_{\ell m}$ of the complex ratio between the PN-expanded $\hat{h}^{(\varepsilon)}_{\ell m}$ and the above defined source and tail factors. In the comparable mass case ($\nu \neq 0$), the f_{22} modulus correction to the leading quadrupolar wave was computed in Ref. [37] (see also Ref. [36] for the $\nu = 0$ limit). For the subleading partial waves, Ref. [50] explicitly computed the other $f_{\ell m}$'s to the highest possible PN-accuracy by starting from the currently known 3PN-accurate ν-dependent waveform [101]. In addition, as originally proposed in Ref. [37], to reach greater accuracy the $f_{\ell m}(x;\nu)$'s extracted from the 3PN-accurate $\nu \neq 0$ results are completed by adding higher order contributions coming from the $\nu = 0$ results [95, 96]. In the particular f_{22} case discussed in [37], this amounted to adding 4PN and 5PN $\nu = 0$ terms. This "hybridization" procedure was then systematically pursued for all the other multipoles, using the 5.5PN accurate calculation of the multipolar decomposition of the gravitational wave energy flux of Refs. [95, 96]. Note that such hybridization procedure is *not* equivalent to the straightforward hybrid sum ansatz,

$\tilde{h}_{\ell m} = \tilde{h}^{\rm known}_{\ell m}(\nu) + \tilde{h}^{\rm higher}_{\ell m}(\nu = 0)$ (where $\tilde{h}_{\ell m} \equiv h_{\ell m}/\nu$) that one may have thought to implement.

In the even-parity case, the determination of the modulus $f_{\ell m}$ is unique. In the odd-parity case, it depends on the choice of the source which, as explained above, can be connected either to the effective energy or to the angular momentum. We will consider both cases and distinguish them by adding either the label H or $\mathscr{J}$ to the corresponding $f_{\ell m}$. Note, in passing, that, since in both cases the factorized effective source term ($H_{\rm eff}$ or $\mathscr{J}$) is a real quantity, the phases $\delta_{\ell m}$'s are the same.

The above explained procedure defines the $f_{\ell m}$'s as Taylor-expanded PN series of the type

$$f_{\ell m}(x;\nu) = 1 + c_1^{f_{\ell m}}(\nu)x + c_2^{f_{\ell m}}(\nu)x^2 + c_3^{f_{\ell m}}(\nu, \log(x))x^3 + \dots \tag{51}$$

Note that one of the virtues of our factorization is to have separated the half-integer powers of x appearing in the usual PN-expansion of $h^{(\varepsilon)}_{\ell m}$ from the integer powers, the tail factor, together with the complementary phase factor $e^{{\rm i}\delta_{\ell m}}$, having absorbed all the half-integer powers. In Ref. [39] all the $f_{\ell m}$'s (both for the H and $\mathscr{J}$ choices) have been computed up to the highest available (ν-dependent or not) PN accuracy. In the formulas for the $f_{\ell m}$'s given below we "hybridize" them by adding to the known ν-dependent coefficients $c_n^{f_{\ell m}}(\nu)$ in Eq. (51) the $\nu = 0$ value of the higher order coefficients: $c_{n'}^{f_{\ell m}}(\nu = 0)$. The 1PN-accurate $f_{\ell m}$'s for $\ell + m$ even and and also for $\ell + m$ odd can be written down for all ℓ. The complete result for the $f_{\ell m}$'s that are known with an accuracy higher than 1PN are listed in Appendix B of Ref. [39]. Here, for illustrative purposes, we quote only the lowest $f^{\rm even}_{\ell m}$ and $f^{{\rm odd},J}_{\ell m}$ up to $\ell = 3$ included.

$$\begin{aligned} f_{22}(x;\nu) &= 1 + \frac{1}{42}(55\nu - 86)x + \frac{\left(2047\nu^2 - 6745\nu - 4288\right)}{1512}x^2 \\ &+ \left(\frac{114635\nu^3}{99792} - \frac{227875\nu^2}{33264} + \frac{41}{96}\pi^2\nu - \frac{34625\nu}{3696} - \frac{856}{105}{\rm eulerlog}_2(x) + \frac{21428357}{727650}\right)x^3 \\ &+ \left(\frac{36808}{2205}{\rm eulerlog}_2(x) - \frac{5391582359}{198648450}\right)x^4 \\ &+ \left(\frac{458816}{19845}{\rm eulerlog}_2(x) - \frac{93684531406}{893918025}\right)x^5 + \mathscr{O}(x^6), \end{aligned} \tag{52}$$

$$\begin{aligned} f^J_{21}(x;\nu) &= 1 + \left(\frac{23\nu}{42} - \frac{59}{28}\right)x + \left(\frac{85\nu^2}{252} - \frac{269\nu}{126} - \frac{5}{9}\right)x^2 \\ &+ \left(\frac{88404893}{11642400} - \frac{214}{105}{\rm eulerlog}_1(x)\right)x^3 \\ &+ \left(\frac{6313}{1470}{\rm eulerlog}_1(x) - \frac{33998136553}{4237833600}\right)x^4 + \mathscr{O}(x^5), \end{aligned} \tag{53}$$

$$f_{33}(x;\nu) = 1 + \left(2\nu - \frac{7}{2}\right)x + \left(\frac{887\nu^2}{330} - \frac{3401\nu}{330} - \frac{443}{440}\right)x^2 + \left(\frac{147471561}{2802800} - \frac{78}{7}\mathrm{eulerlog}_3(x)\right)x^3 + \left(39\,\mathrm{eulerlog}_3(x) - \frac{53641811}{457600}\right)x^4 + \mathscr{O}(x^5), \tag{54}$$

$$f^J_{32}(x;\nu) = 1 + \frac{320\nu^2 - 1115\nu + 328}{90(3\nu-1)}x + \frac{39544\nu^3 - 253768\nu^2 + 117215\nu - 20496}{11880(3\nu-1)}x^2 + \left(\frac{110842222}{4729725} - \frac{104}{21}\mathrm{eulerlog}_2(x)\right)x^3 + \mathscr{O}(x^4), \tag{55}$$

$$f_{31}(x;\nu) = 1 + \left(-\frac{2\nu}{3} - \frac{13}{6}\right)x + \left(-\frac{247\nu^2}{198} - \frac{371\nu}{198} + \frac{1273}{792}\right)x^2 + \left(\frac{400427563}{75675600} - \frac{26}{21}\mathrm{eulerlog}_1(x)\right)x^3 + \left(\frac{169}{63}\mathrm{eulerlog}_1(x) - \frac{12064573043}{1816214400}\right)x^4 + \mathscr{O}(x^5). \tag{56}$$

For convenience and readability, we have introduced the following "eulerlog" functions $\mathrm{eulerlog}_m(x)$ $\mathrm{eulerlog}_m(x) = \gamma_E + \log 2 + \frac{1}{2}\log x + \log m$, where $\gamma_E = 0.57721\ldots$ is Euler's constant.

The decomposition of the total PN-correction factor $\hat{h}^{(\varepsilon)}_{\ell m}$ into several factors is in itself a resummation procedure which has already improved the convergence of the PN series one has to deal with: indeed, one can see that the coefficients entering increasing powers of x in the $f_{\ell m}$'s tend to be systematically smaller than the coefficients appearing in the usual PN expansion of $\hat{h}^{(\varepsilon)}_{\ell m}$. The reason for this is essentially twofold: (i) the factorization of $T_{\ell m}$ has absorbed powers of $m\pi$ which contributed to make large coefficients in $\hat{h}^{(\varepsilon)}_{\ell m}$, and (ii) the factorization of either $\hat{H}_{\rm eff}$ or $\hat{j}$ has (in the $\nu = 0$ case) removed the presence of an inverse square-root singularity located at $x = 1/3$ which caused the coefficient of x^n in any PN-expanded quantity to grow as 3^n as $n \to \infty$. To prevent some potential misunderstandings, let us emphasize that we are talking here about a singularity entering the analytic continuation (to larger values of x) of a mathematical function $h(x)$ defined (for small values of x) by considering the formal adiabatic circular limit. The point is that, in the $\nu \to 0$ limit, the radius of convergence and therefore the growth with n of the PN coefficients of $h(x)$ (Taylor-expanded at $x = 0$), are linked to the singularity of the analytically continued $h(x)$ which is nearest to $x = 0$ in the complex x-plane. In the $\nu \to 0$ case, the nearest singularity in the complex x-plane comes from the source factor $\hat{H}_{\rm eff}(x)$ or $\hat{j}(x)$ in the waveform and is located at the light-ring $x_{\rm LR}(\nu = 0) = 1/3$. In the $\nu \neq 0$ case, the EOB formalism transforms the latter (inverse square-root) singularity in a more complicated ("branching") singularity where $d\hat{H}_{\rm eff}/dx$ and $d\hat{j}/dx$ have inverse square-root singularities located at what

is called [3, 31, 33, 38, 37] the (Effective)[12] "EOB-light-ring", i.e., the (adiabatic) maximum of Ω, $x_{\rm ELR}^{\rm adiab}(\nu) \equiv \left(M\Omega_{\rm max}^{\rm adiab}\right)^{2/3} \gtrsim 1/3$.

Despite this improvement, the resulting "convergence" of the usual Taylor-expanded $f_{\ell m}(x)$'s quoted above does not seem to be good enough, especially near or below the LSO, in view of the high-accuracy needed to define gravitational wave templates. For this reason, Refs. [36, 37] proposed to further resum the $f_{22}(x)$ function via a Padé (3,2) approximant, $P_2^3\{f_{22}(x;\nu)\}$, so as to improve its behavior in the strong-field-fast-motion regime. Such a resummation gave an excellent agreement with numerically computed waveforms, near the end of the inspiral and during the beginning of the plunge, for different mass ratios [36, 38, 39]. As we were mentioning above, a new route for resumming $f_{\ell m}$ was explored in Ref. [50]. It is based on replacing $f_{\ell m}$ by its ℓ-th root, say

$$\rho_{\ell m}(x;\nu) = [f_{\ell m}(x;\nu)]^{1/\ell}. \tag{57}$$

The basic motivation for replacing $f_{\ell m}$ by $\rho_{\ell m}$ is the following: the leading "Newtonian-level" contribution to the waveform $h_{\ell m}^{(\varepsilon)}$ contains a factor $\omega^\ell r_{\rm harm}^\ell v^\varepsilon$ where $r_{\rm harm}$ is the harmonic radial coordinate used in the MPM formalism [66, 68] . When computing the PN expansion of this factor one has to insert the PN expansion of the (dimensionless) harmonic radial coordinate $r_{\rm harm}$, $r_{\rm harm} = x^{-1}(1 + c_1 x + \mathcal{O}(x^2))$, as a function of the gauge-independent frequency parameter x. The PN re-expansion of $[r_{\rm harm}(x)]^\ell$ then generates terms of the type $x^{-\ell}(1 + \ell c_1 x + ...)$. This is one (though not the only one) of the origins of 1PN corrections in $h_{\ell m}$ and $f_{\ell m}$ whose coefficients grow linearly with ℓ. The study of [50] has pointed out that these ℓ-growing terms are problematic for the accuracy of the PN-expansions. Our replacement of $f_{\ell m}$ by $\rho_{\ell m}$ is a cure for this problem. More explicitly, the the investigation of 1PN corrections to GW amplitudes [66, 68, 99] has shown that, in the even-parity case (but see also Appendix A of Ref. [50] for the odd-parity case),

$$c_1^{f_{\ell m}}(\nu) = -\ell\left(1 - \frac{\nu}{3}\right) + \frac{1}{2} + \frac{3}{2}\frac{c_{\ell+2}(\nu)}{c_\ell(\nu)} - \frac{b_\ell(\nu)}{c_\ell(\nu)} - \frac{c_{\ell+2}(\nu)}{c_\ell(\nu)}\frac{m^2(\ell+9)}{2(\ell+1)(2\ell+3)}, \tag{58}$$

where $c_\ell(\nu)$ is defined in Eq. (45) and

$$b_\ell(\nu) \equiv X_2^\ell + (-)^\ell X_1^\ell. \tag{59}$$

Focusing on the $\nu = 0$ case for simplicitly (since the ν dependence of $c_1^{f_{\ell m}}(\nu)$ is quite mild [50]), the above result shows that the PN expansion of $f_{\ell m}$ starts as

$$f_{\ell m}^{\rm even}(x;0) = 1 - \ell x\left(1 - \frac{1}{\ell} + \frac{m^2(\ell+9)}{2\ell(\ell+1)(2\ell+3)}\right) + \mathcal{O}(x^2). \tag{60}$$

[12] Beware that this "Effective EOB-light-ring" occurs for a circular-orbit radius slightly larger than the purely dynamical (circular) EOB-light-ring (where $H_{\rm eff}$ and $\mathscr{J}$ would formally become infinite).

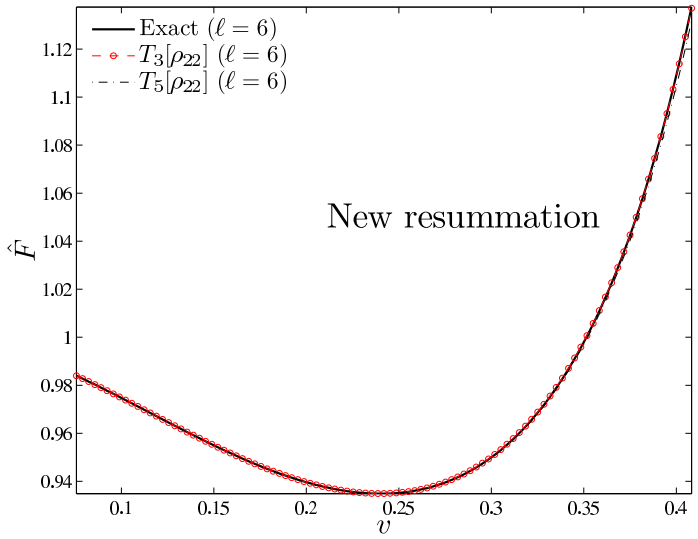

Fig. 6 Performance of the new resummation procedure described in Ref. [50]. The total GW flux $\hat{F}$ (up to $\ell_{\rm max} = 6$) computed from inserting in Eq. (62) the factorized waveform (41) with the Taylor-expanded $\rho_{\ell m}$'s (with either 3PN or 5PN accuracy for ρ_{22}) is compared with the "exact" numerical data.

The crucial thing to note in this result is that as ℓ gets large (keeping in mind that $|m| \leq \ell$), the coefficient of x will be negative and will approximately range between $-5\ell/4$ and $-\ell$. This means that when $\ell \geq 6$ the 1PN correction in $f_{\ell m}$ would by itself make $f_{\ell m}(x)$ vanish before the ($\nu = 0$) LSO $x_{\rm LSO} = 1/6$. For example, for the $\ell = m = 6$ mode, one has $f_{66}^{\rm 1PN}(x;0) = 1 - 6x(1 + 11/42) \approx 1 - 6x(1 + 0.26)$ which means a correction equal to -100% at $x = 1/7.57$ and larger than -100% at the LSO, namely $f_{66}^{\rm 1PN}(1/6;0) \approx 1 - 1.26 = -0.26$. This value is totally incompatible with the "exact" value $f_{22}^{\rm exact}(x_{\rm LSO}) = 0.66314511$ computed from numerical data in Ref. [50].

Finally, one uses the newly resummed multipolar waveforms (41) to define a resummation of the *radiation reaction force* $\mathscr{F}_\varphi$ is defined as

$$\mathscr{F}_\varphi = -\frac{1}{\Omega} F^{(\ell_{\rm max})}, \tag{61}$$

where the (instantaneous, circular) GW flux $F^{(\ell_{\rm max})}$ is defined as

$$F^{(\ell_{\rm max})} = \frac{2}{16\pi G} \sum_{\ell=2}^{\ell_{\rm max}} \sum_{m=1}^{\ell} |R\dot{h}_{\ell m}|^2 = \frac{2}{16\pi G} \sum_{\ell=2}^{\ell_{\rm max}} \sum_{m=1}^{\ell} (m\Omega)^2 |Rh_{\ell m}|^2. \tag{62}$$

As an example of the performance of the new resummation procedure based on the decomposition of $h_{\ell m}$ given by Eq. (41), let us focus, as before, on the computation of the GW energy flux emitted by a test particle on circular orbits on Schwarzschild

spacetime. Figure 6 illustrates the remarkable improvement in the closeness between $\hat{F}^{\rm New\text{-}resummed}$ and $\hat{F}^{\rm Exact}$. The reader should compare this result with the previous Fig. 3 (the straightforward Taylor approximants to the flux), Fig. 4 (the Padé resummation with $\nu_{\rm pole}=1/\sqrt{3}$) and Fig. 5 (the $\nu_{\rm pole}$-tuned Padé resummation). To be fully precise, Fig. 6 plots two examples of fluxes obtained from our new $\rho_{\ell m}$-representation for the individual multipolar waveforms $h_{\ell m}$. These two examples differ in the choice of approximants for the $\ell=m=2$ partial wave. One example uses for ρ_{22} its 3PN Taylor expansion, $T_3[\rho_{22}]$, while the other one uses its 5PN Taylor expansion, $T_5[\rho_{22}]$. All the other partial waves are given by their maximum known Taylor expansion[13]. Note that the fact that we use here for the $\rho_{\ell m}$'s some straightforward Taylor expansions does not mean that this new procedure is not a resummation technique. Indeed, the defining resummation features of our procedure have four sources: (i) the factorization of the PN corrections to the waveforms into four different blocks, namely $\hat{S}^{(\varepsilon)}_{\rm eff}$, $T_{\ell m}$, $e^{{\rm i}\delta_{\ell m}}$ and $\rho^{\ell}_{\ell m}$ in Eq. (41); (ii) the fact the $\hat{S}^{(\varepsilon)}_{\rm eff}$ is by itself a resummed source whose PN expansion would contain an infinite number of terms; (iii) the fact that the tail factor is a closed form expression (see Eq. (50) above) whose PN expansion also contains an infinite number of terms and (iv) the fact that we have replaced the Taylor expansion of $f_{\ell m}\equiv\rho^{\ell}_{\ell m}$ by that of its ℓ-th root, namely $\rho_{\ell m}$.

In conclusion, Eqs. (41) and (62) introduce a new recipe to resum the (ν-dependent) GW energy flux that is alternative to the ($\nu_{\rm pole}$-tuned) one given by Eq. (40). The two main advantages of the new resummation are: (i) it gives a better representation of the exact result in the $\nu\to 0$ limit (compare Fig. 6 to Fig. 5), and (ii) it is *parameter-free*: the only flexibility that one has in the definition of the waveform and flux is the choice of the analytical representation of the function f_{22}, like, for instance, $P^3_2\{f_{22}\}$, $(T_3[\rho_{22}])^2$, $(T_5[\rho_{22}])^2$, etc., (although Ref. [50] has pointed out the good consistency among all these choices). Note, that when $\nu\neq 0$, the GW energy flux will depend on the choice of resummation of the radial potential $A(R)$ through the Hamiltonian (for the even-parity modes) or the angular momentum (for the odd-parity modes). At the practical level, this means that the EOB model, implemented with the new resummation procedure of the energy flux (and waveform) described so far, will essentially only depend on the doublet of parameters (a_5,a_6), that can in principle be constrained by comparison with (accurate) numerical relativity results. Contrary to the previous $\nu_{\rm pole}$-resummation of the radiation reaction, this route to resummation is free of radiation-reaction flexibility parameters. We will consider it as our "standard" route to the resummation of the energy flux in the following Sections discussing in details the properties of the EOB dynamics and waveforms.

[13] We recall that Ref. [50] has also shown that the agreement improves even more when the Taylor expansion of the function ρ_{22} is further suitably Padé resummed.

5 Effective One Body dynamics and waveforms

In this section we marry together all the EOB building blocks described in the previous Sections and discuss the characteristic of the dynamics of the two black holes as provided by the EOB approach. In the following three subsections we discuss in some detail: (i) the set up of initial data for the EOB dynamics with negligible eccentricity (Sec. 5.1); (ii) the structure of the full Effective One Body waveform, covering inspiral, plunge, merger and ringdown, with the introduction of suitable Next-to-Quasi-Circular (NQC) effective corrections to it (and thus to the energy flux) (Sec. 5.2); (iii) the explicit structure of the EOB dynamics, discussing the solution of the dynamical equations.

5.1 Post-post-circular initial data

In this section we discuss in detail the so-called *post-post-circular* dynamical initial data (positions and momenta) as introduced in Sec. III B of [37]. This kind of (improved) construction is needed to have initial data with negligible eccentricity. Since the construction of the initial data is analytical, including the correction is useful to start the system relatively close and to avoid evolving the EOB equation of motion for a long time in order to make the system circularize itself.

To explain the improved construction of initial data let us introduce a formal book-keeping parameter ε (to be set to 1 at the end) in front of the radiation reaction $\hat{\mathscr{F}}_\varphi$ in the EOB equations of motion. One can then show that the quasi-circular inspiralling solution of the EOB equations of motion formally satisfies

$$p_\varphi = j_0(r) + \varepsilon^2 j_2(r) + O(\varepsilon^4), \tag{63}$$

$$p_{r_*} = \varepsilon\pi_1(r) + \varepsilon^3\pi_3(r) + O(\varepsilon^5). \tag{64}$$

Here, $j_0(r)$ is the usual *circular* approximation to the inspiralling angular momentum as explicitly given by Eq. (47) above. The order ε ("post-circular") term $\pi_1(r)$ is obtained by: (i) inserting the circular approximation $p_\varphi = j_0(r)$ on the left-hand side (l.h.s) of Eq. (10) of [34], (ii) using the chain rule $dj_0(r)/dt = (dj_0(r)/dr)(dr/dt)$, (iii) replacing dr/dt by the right-hand side (r.h.s) of Eq. (9) of [34] and (iv) solving for p_{r_*} at the first order in ε. This leads to an explicit result of the form (using the notation defined in Ref. [34])

$$\varepsilon\pi_1(r) = \left[v\hat{H}\hat{H}_{\rm eff} \left(\frac{B}{A}\right)^{1/2} \left(\frac{dj_0}{dr}\right)^{-1} \hat{\mathscr{F}}_\varphi \right]_0 , \tag{65}$$

where the subscript 0 indicates that the r.h.s. is evaluated at the leading circular approximation $\varepsilon \to 0$. The post-circular EOB approximation (j_0, π_1) was introduced in Ref. [3] and then used in most of the subsequent EOB papers [6, 31,

32, 33, 34, 35]. The *post-post-circular* approximation (order ε^2), introduced in Ref. [37] and then used systematically in Ref. [38, 39, 40], consists of: (i) formally solving Eq. (35) with respect to the explicit p_φ^2 appearing on the r.h.s., (ii) replacing p_{r_*} by its post-circular approximation, Eq. (65), (iii) using the chain rule $d\pi_1(r)/dt = (d\pi_1(r)/dr)(dr/dt)$, and (iv) replacing dr/dt in terms of π_1 (to leading order) by using Eq. (33). The result yields an explicit expression of the type $p_\varphi^2 \simeq j_0^2(r)[1+\varepsilon^2 k_2(r)]$ of which one finally takes the square root. In principle, this procedure can be iterated to get initial data at any order in ε. As it will be shown below, the post-post-circular initial data $(j_0\sqrt{1+\varepsilon^2 k_2}, \pi_1)$ are sufficient to lead to negligible eccentricity when starting the integration of the EOB equations of motion at radius $r \equiv R/(GM) = 15$.

5.2 Effective One Body waveforms

At this stage we have essentially discussed all the elements that are needed to compute the EOB dynamics obtained by solving the EOB equation of motion, Eqs. (32)-(35). The dynamics of the system yields a trajectory $(\boldsymbol{q}(t), \boldsymbol{p}(t)) \equiv (\varphi(t), r(t), p_\varphi(t), p_{r_*}(t))$ in phase space. The (multipolar) metric waveform during the inspiral and plunge phase, up to the EOB "merger time" t_m (that is defined as the maximum of the orbital frequency Ω,) is a function of this trajectory, i.e. $h_{\ell m}^{\rm insplunge} \equiv h_{\ell m}^{\rm insplunge}(\boldsymbol{q}(t), \boldsymbol{p}(t))$. Focusing only on the dominant $\ell = m = 2$ waveform, the waveform that describes the full process of the binary black hole coalescence (i.e., inspiral, plunge, merger and ringdown) can be split in two parts:

- The *insplunge waveform*: $h^{\rm insplunge}(t)$, computed along the EOB dynamics up to merger, which includes (i) the resummation of the "tail" terms described above and (ii) some effective parametrization of Next-to-Quasi-Circular effects. The $\ell = m = 2$ metric waveform explicitly reads

$$\left(\frac{Rc^2}{GM}\right) h_{22}^{\rm insplunge}(t) = \nu n_{22}^{(0)} c_2(\nu) x \hat{h}_{22}(\nu; x) f_{22}^{\rm NQC} Y^{2,-2}\left(\frac{\pi}{2}, \Phi\right), \qquad (66)$$

  where the argument x is taken to be (following [90]) $x = v_\varphi^2 = (r_\omega \Omega)^2$ (where r_ω was introduced in Eq. (36) above). The resummed version of f_{22} entering in $\hat{h}_{22}(x)$ used here is given by the following *Padé-resummed* function $f_{22}^{\rm Pf} \equiv P_2^3[f_{22}^{\rm Taylor}(x;\nu)]$. In the waveform h_{22} above we have introduced (following [40]) a new ingredient, a "Next-to-Quasi-Circular" (NQC) correction factor of the form[14]

$$f_{22}^{\rm NQC}(a_1, a_2) = 1 + a_1 \frac{p_{r_*}^2}{(r\Omega)^2} + a_2 \frac{\ddot{r}}{r\Omega^2}, \qquad (67)$$

[14] Note that one could also similarly improve the subleading higher-multipolar-order contributions to $\mathscr{F}_\varphi$. In addition, other (similar) expressions of the NQC factors can be found in the literature [38, 39, 41].

where a_1 and a_2 are free parameters that have to be fixed. A crucial facet of the new EOB formalism presented here consists in trying to be as predictive as possible by reducing to an absolute minimum the number of "flexibility parameters" entering our theoretical framework. One can achieve this aim by "analytically" determining the two parameters a_1, a_2 entering (via the NQC factor Eq. (67)) the (asymptotic) quadrupolar EOB waveform $\hat{R}h_{22}^{\rm EOB}$ (where $\hat{R} = R/M$) by imposing: (a) that the modulus $|\hat{R}h_{22}^{\rm EOB}|$ reaches, at the EOB-determined "merger time" t_m, a *local maximum*, and (b) that the value of this maximum EOB modulus is equal to a certain (dimensionless) function of ν, $\varphi(\nu)$. In Ref. [40] we calibrated $\varphi(\nu)$ (independently of the EOB formalism) by extracting from the best current Numerical Relativity simulations the maximum value of the modulus of the Numerical Relativity quadrupolar *metric* waveform $|\hat{R}h_{22}^{\rm NR}|$. Using the data reported in [29] and [39], and considering the "Zerilli-normalized" asymptotic metric waveform $\Psi_{22} = \hat{R}h_{22}/\sqrt{24}$, we found $\varphi(\nu) \simeq 0.3215\nu(1-0.131(1-4\nu))$. Our requirements (a) and (b) impose, for any given $A(u)$ potential, *two constraints* on the *two parameters* a_1, a_2. We can solve these two constraints (by an iteration procedure) and thereby uniquely determine the values of a_1, a_2 corresponding to any given $A(u)$ potential. In particular, in the case considered here where $A(u) \equiv A(u; a_5, a_6, \nu)$ this uniquely determines a_1, a_2 in function of a_5, a_6 and ν. Note that this is done while also consistently using the "improved" version of h_{22} given by Eq. (66) to compute the radiation reaction force via Eq. (62).

- a simplified representation of the transition between plunge and ring-down by smoothly *matching* (following Refs. [36]), on a $(2p+1)$-toothed "comb" $(t_m - p\delta, \ldots, t_m - \delta, t_m, t_m + \delta, \ldots, t_m + p\delta)$ centered around a matching time t_m, the inspiral-plus-plunge waveform to a ring-down waveform, made of the superposition of several[15] quasi-normal-mode complex frequencies,

$$\left(\frac{Rc^2}{GM}\right) h_{22}^{\rm ringdown}(t) = \sum_N C_N^+ \, e^{-\sigma_N^+ (t-t_m)} \,, \tag{68}$$

with $\sigma_N^+ = \alpha_N + i\,\omega_N$, and where the label N refers to indices (ℓ, ℓ', m, n), with $(\ell, m) = (2,2)$ being the Schwarzschild-background multipolarity of the considered (metric) waveform $h_{\ell m}$, with $n = 0, 1, 2 \ldots$ being the 'overtone number' of the considered Kerr-background Quasi-Normal-Mode, and ℓ' the degree of its associated spheroidal harmonics $S_{\ell' m}(a\sigma, \theta)$. As discussed in [3] and [36], and already mentioned above, the physics of the transition between plunge and ring-down (which was first understood in the classic work of Davis, Ruffini and Tiomno [51]) suggests to choose as matching time t_m, in the comparable-mass case, the EOB time when the EOB orbital frequency $\Omega(t)$ reaches its *maximum* value.

Finally, one defines a complete, quasi-analytical EOB waveform (covering the full process from inspiral to ring-down) as:

[15] Refs. [36, 38] use $p = 2$, *i.e.* a 5-teethed comb, and, correspondingly, 5 positive-frequency Kerr Quasi-Normal Modes.

$$h_{22}^{\rm EOB}(t) = \theta(t_m - t)\, h_{22}^{\rm insplunge}(t) + \theta(t - t_m)\, h_{22}^{\rm ringdown}(t)\,, \tag{69}$$

where $\theta(t)$ denotes Heaviside's step function. The final result is a waveform that only depends on the *two* parameters (a_5, a_6) which parametrize some flexibility on the Padé resummation of the basic radial potential $A(u)$, connected to the yet uncalculated (4PN, 5PN and) higher PN contributions.

5.3 Effective One Body dynamics

We conclude this section by discussing the features of the typical EOB dynamics obtained by solving the EOB equation of motion Eqs. (32)-(35) with post-post-circular initial data. The resummation of the radiation reaction force uses the multiplicative decomposition of $h_{\ell m}$ given by Eq. (41) with NQC correction to the $\ell = m = 2$ multipole given by Eq. (67). We fix the free parameters to the model to be $a_5 = 0$, $a_6 = -20$ (see below why) while a_1 and a_2 are obtained consistently according to the iteration procedure discussed above. The system is started at $r_0 = 15$ and $\varphi_0 = 0$. The post-post-circular initial data give $p_\varphi^0 = 4.31509298$ and $p_{r_*}^0 = -0.00109847$. The result of the outcome of the integration of the EOB equation of motion is displayed in Fig. 7 together with the trajectory (top-left panel) and the orbital frequency (bottom-right panel). On this plot we remark two things. First, the fact that the orbital frequency has a maximum at time $t_m = 3522$ that identifies, in EOB, the merger (and matching) time. Second, the fact that p_{r_*} tends to a finite value after the merger (contrary to p_r, that would diverge), yielding a more controllable numerical treatment of the late part of the EOB dynamics.

6 Effective One Body and Numerical Relativity waveforms

So far we have seen that (at least) two different EOB models (of dynamics and waveforms) are available. They differ, essentially, in the way the resummation of the GW energy flux yielding the radiation reaction force is performed. The first EOB model, that we will refer to as the "old" one, basically uses a Padé-resummation of the energy flux with an external parameter $v_{\rm pole}$ that must be fixed in some way. The second EOB model, that we will refer to as the "improved" one, uses a more sophisticated resummation procedure of the energy flux, multipole by multipole, in such a way that the final result depends explicitly only on the same parameters (a_5, a_6) that are used to parametrize higher PN contribution to the conservative part of the dynamics.

In the last three years, the power of the "old" EOB model has been exploited in various comparisons with numerical relativity data, aiming at constraining in some way the space of the EOB flexibility parameters (notably represented by a_5 and $v_{\rm pole}$) by looking at regions in the parameter space where the agreement between the

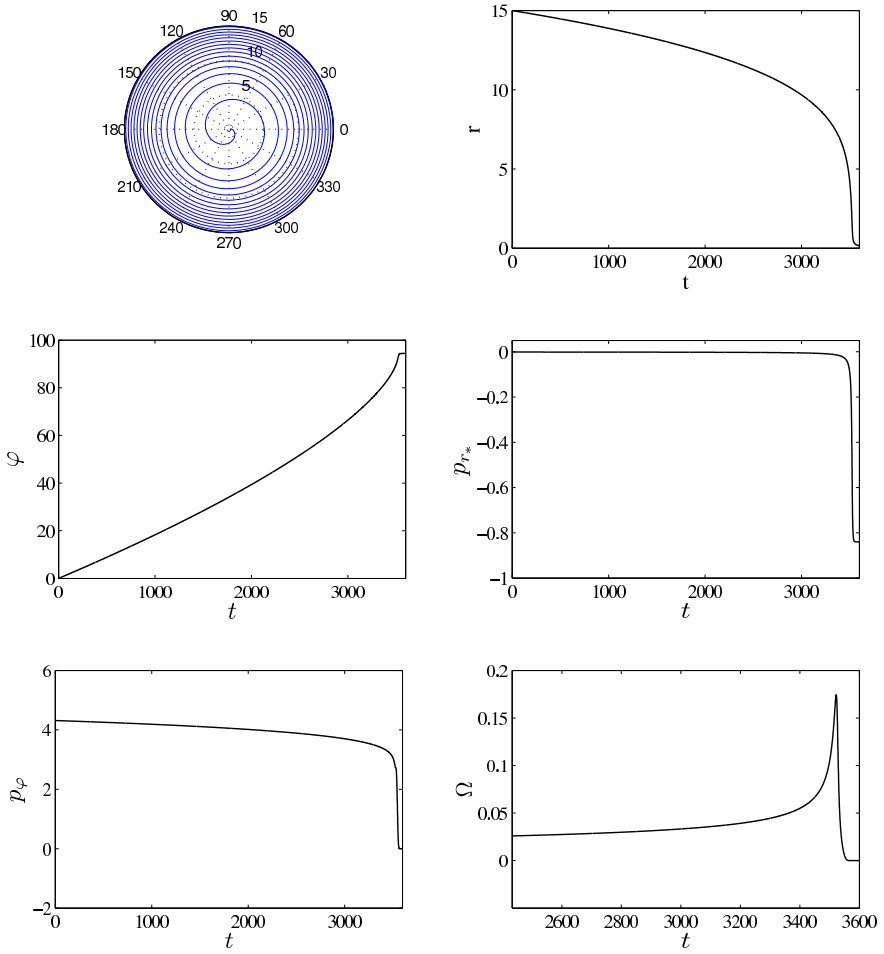

Fig. 7 EOB dynamics for $a_5 = 0$ and $a_6 = -20$. Clockwise from the top left panel,the panels report: the trajectory, the radial separation $r(t)$, the radial momentum p_{r_*} (conjugate to r_*), the orbital frequency $\Omega(t)$, the angular momentum $p_\varphi(t)$ and the orbital phase $\varphi(t)$.

numerical and analytical waveforms is at the level of numerical error. For example, after a preliminary comparison done in Ref. [31], Buonanno et al. [33] compared *restricted* EOB waveforms[16] to NR waveforms computed by the NASA-Goddard group, showing that it is possible to tune the value of a_5 so as to have a good agreement between the two set of data. In particular, for $a_5 = 60$ and $\nu_{\rm pole}$ given according to the (nowadays outdated) suggestion of Ref. [49], in the equal-mass case ($\nu = 1/4$), they found that the dephasing between (restricted) EOB and NR waveforms (covering late inspiral, merger and ring-down) stayed within ± 0.030

[16] The terminology "restricted" refers to a waveform which uses only the leading *Newtonian* approximation, $h_{\ell m}^{(N,\varepsilon)}$, to the waveform

GW cycles over 14 GW cycles. In the case of a mass ratio $4:1$ ($\nu = 0.16$), the dephasing stayed within ± 0.035 GW cycles over 9 GW cycles.

Later, the *resummed* factorized EOB waveform of Eq. (66) above within the "old" EOB model has been compared to several set of equal-mass and unequal-mass NR waveforms: (i) in the comparison with the very accurate inspiralling simulation of the Caltech-Cornell group [27] the dephasing stayed smaller than ± 0.001 GW cycles over 30 GW cycles (and the amplitudes agreed at the $\sim 10^{-3}$ level) [37]; (ii) in the comparison [38] with a late-inspiral-merger-ringdown NR waveform computed by the Albert Einstein Institute group, the dephasing stayed smaller than ± 0.005 GW cycles over 12 GW cycles; (iii) in the (joint) comparison [39] between EOB and very accurate equal-mass inspiralling simulation of the Caltech-Cornell group [27] and late-inspiral-merger-ringdown waveform for 1:1, 2:1 and 4:1 mass ratio data computed by the Jena group it was possible to tune the EOB flexibility parameters (notably a_5 and $v_{\rm pole}$) so that the dephasing stayed at the level of the numerical error. The same "old" model, with resummed factorized waveform, and the parameter-dependent (using $v_{\rm pole}$) resummation of radiation reaction force, was recently extended by adding 6 more flexibility parameters to the ones already intrduced in Refs. [37, 39], and was "calibrated" on the high-accuracy Caltech-Cornell equal-mass data [41]. This calibration showed that only 5 flexibility parameters (a_5, $v_{\rm pole}$ and three parameters related to non-quasi-circular corrections to the waveform amplitude) actually suffice to make the "old" EOB and NR waveform agree, both in amplitude and phase, at the level of the numerical error (this multi-flexed EOB model brings in an improvement with respect to the one of Refs. [37, 39] especially for what concerns the agreement between the waveform amplitude around the merger).

Recently, Ref. [40] has introduced and fully exploited the possibilities of the "improved" EOB formalism described above, taking advantage of: (i) the multiplicative decomposition of the (resummed) multipolar waveform advocated in Eq. (41) above, (ii) the effect of the NQC corrections to the waveform (and energy flux) given by Eq. (66), and, most importantly, (iii) the parameter-free resummation of radiation reaction $\mathscr{F}_\varphi$. In Ref. [40] the (a_5, a_6)-dependent predictions made by the "improved" formalism were compared to the high-accuracy waveform from an equal-mass BBH ($\nu = 1/4$) computed by the Caltech-Cornell group [29], (and now made available on the web). It was found that there is a strong degeneracy between a_5 and a_6 in the sense that there is an excellent EOB-NR agreement for an extended region in the (a_5, a_6)-plane. More precisely, the phase difference between the EOB (metric) waveform and the Caltech-Cornell one, considered between GW frequencies $M\omega_{\rm L} = 0.047$ and $M\omega_{\rm R} = 0.31$ (i.e., the last 16 GW cycles before merger), stays smaller than 0.02 radians within a long and thin banana-like region in the (a_5, a_6)-plane. This "good region" approximately extends between the points $(a_5, a_6) = (0, -20)$ and $(a_5, a_6) = (-36, +520)$. As an example (which actually lies on the boundary of the "good region"), we have followed [40] in considering here the specific values $a_5 = 0, a_6 = -20$ (to which correspond, when $\nu = 1/4$, $a_1 = -0.036347, a_2 = 1.2468$). We henceforth use M as time unit.

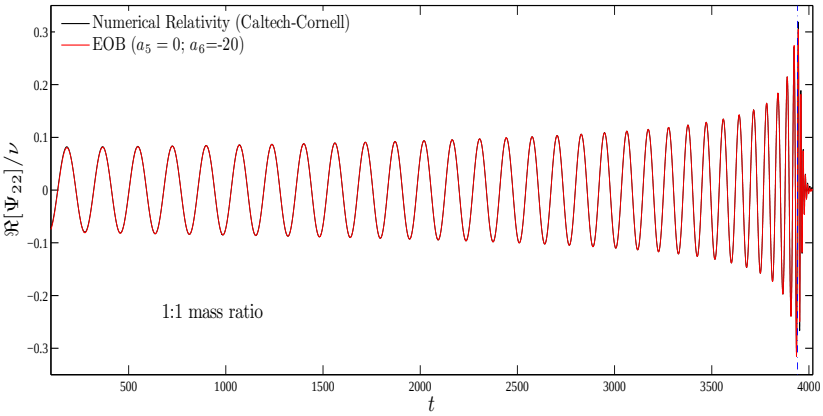

Fig. 8 This figure illustrates the comparison between the "improved" EOB waveform (quadrupolar ($\ell = m = 2$) metric waveform (66) with parameter-free radiation reaction (61) and with $a_5 = 0$,$a_6 = -20$) with the most accurate numerical relativity waveform (equal-mass case) nowadays available. The phase difference between the two is $\Delta\phi \leq \pm 0.01$ radians during the entire inspiral and plunge. Ref. [40] has shown that this agreement is at the level of the numerical error.

This result relies on the proper comparison between NR and EOB time series, which is a delicate subject. In fact, to compare the NR and EOB phase time-series $\phi_{22}^{\rm NR}(t_{\rm NR})$ and $\phi_{22}^{\rm EOB}(t_{\rm EOB})$ one needs to shift, by additive constants, both one of the time variables, and one of the phases. In other words, we need to determine τ and α such that the "shifted" EOB quantities

$$t'_{\rm EOB} = t_{\rm EOB} + \tau\,, \quad \phi_{22}^{\prime\rm EOB} = \phi_{22}^{\rm EOB} + \alpha \tag{70}$$

"best fit" the NR ones. One convenient way to do so is first to "pinch" the EOB/NR phase difference at two different instants (corresponding to two different frequencies). More precisely, one can choose two NR times $t_1^{\rm NR}, t_2^{\rm NR}$, which determine two corresponding GW frequencies[17] $\omega_1 = \omega_{22}^{\rm NR}(t_1^{\rm NR})$, $\omega_2 = \omega_{22}^{\rm NR}(t_2^{\rm NR})$, and then find the time shift $\tau(\omega_1,\omega_2)$ such that the shifted EOB phase difference, between ω_1 and ω_2, $\Delta\phi^{\rm EOB}(\tau) \equiv \phi_{22}^{\prime\rm EOB}(t_2^{\prime\rm EOB}) - \phi_{22}^{\prime\rm EOB}(t_1^{\prime\rm EOB}) = \phi_{22}^{\rm EOB}(t_2^{\rm EOB}+\tau) - \phi_{22}^{\rm EOB}(t_1^{\rm EOB}+\tau)$ is equal to the corresponding (unshifted) NR phase difference $\Delta\phi^{\rm NR} \equiv \phi_{22}^{\rm NR}(t_2^{\rm NR}) - \phi_{22}^{\rm NR}(t_1^{\rm NR})$. This yields one equation for one unknown (τ), and (uniquely) determines a value $\tau(\omega_1,\omega_2)$ of τ. [Note that the $\omega_2 \to \omega_1 = \omega_m$ limit of this procedure yields the one-frequency matching procedure used in [27].] After having so determined τ, one can uniquely define a corresponding best-fit phase shift $\alpha(\omega_1,\omega_2)$ by requiring that, say, $\phi_{22}^{\prime\rm EOB}(t_1^{\prime\rm EOB}) \equiv \phi_{22}^{\rm EOB}(t_1^{\prime\rm EOB}) + \alpha = \phi_{22}^{\rm NR}(t_1^{\rm NR})$.

[17] Alternatively, one can start by giving oneself ω_1,ω_2 and determine the NR instants $t_1^{\rm NR}, t_2^{\rm NR}$ at which they are reached.

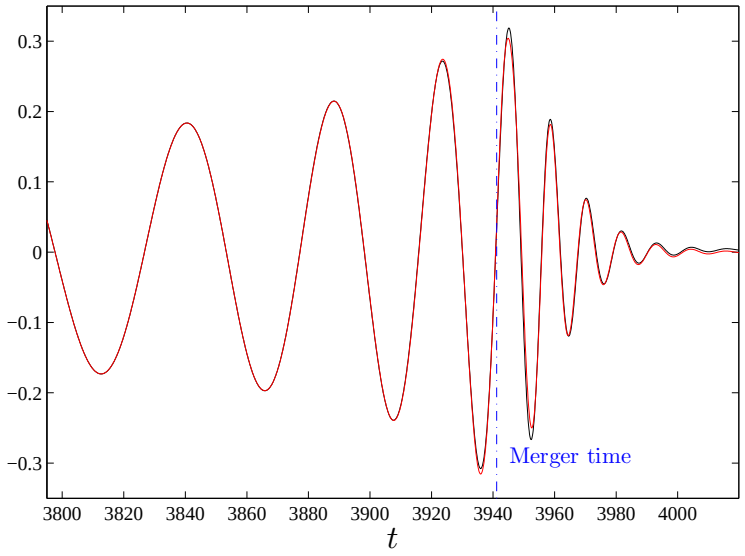

Fig. 9 Close up around merger of the waveforms of Fig. 8. Note the excellent agreement between *both* modulus and phasing also during the ringdown phase.

Having so related the EOB time and phase variables to the NR ones we can straigthforwardly compare all the EOB time series to their NR correspondants. In particular, we can compute the (shifted) EOB–NR phase difference

$$\Delta^{\omega_1,\omega_2}\phi_{22}^{\rm EOBNR}(t_{\rm NR}) \equiv \phi_{22}^{\prime\rm EOB}(t^{\prime\rm EOB}) - \phi_{22}^{\rm NR}(t^{\rm NR}). \tag{71}$$

Figure 8 compares[18] (the real part of) our analytical *metric* quadrupolar waveform $\Psi_{22}^{\rm EOB}/\nu$ to the corresponding (Caltech-Cornell) NR *metric* waveform $\Psi_{22}^{\rm NR}/\nu$. This NR metric waveform has been obtained by a double time-integration (following the procedure of Ref. [39]) from the original, publicly available, *curvature* waveform ψ_4^{22}. Such a curvature waveform has been extrapolated *both* in resolution and in extraction radius. The agreement between the analytical prediction and the NR result is striking, even around the merger. See Fig. 9 which closes up on the merger. The vertical line indicates the location of the EOB-merger time, i.e., the location of the maximum of the orbital frequency.

The phasing agreement between the waveforms is excellent over the full time span of the simulation (which covers 32 cycles of inspiral and about 6 cycles of ringdown), while the modulus agreement is excellent over the full span, apart from two cycles after merger where one can notice a difference. More precisely, the phase

[18] The two frequencies used for this comparison, by means of the "two-frequency pinching technique" mentioned above, are $M\omega_1 = 0.047$ and $M_{\omega_2} = 0.31$.

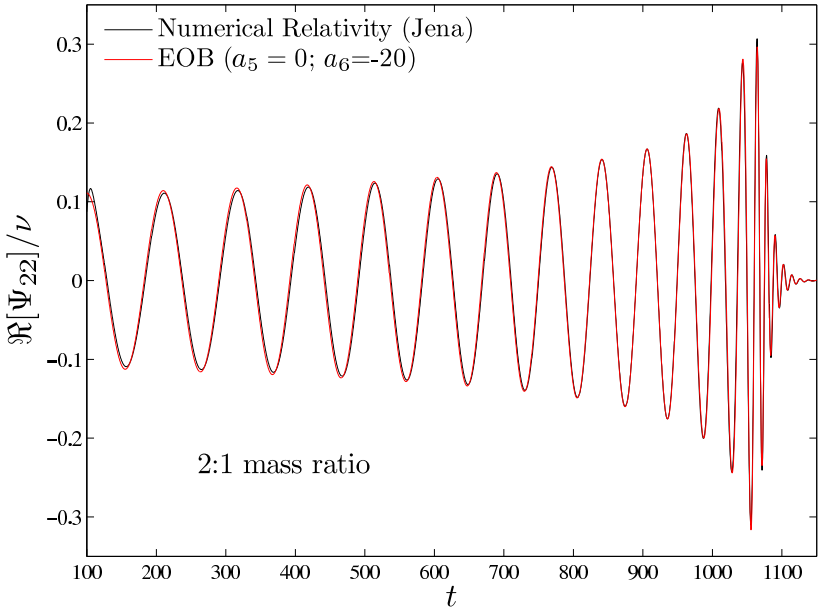

Fig. 10 Comparison between Numerical Relativity and EOB metric waveform for the 2:1 mass ratio.

difference, $\Delta\phi = \phi^{\rm EOB}_{\rm metric} - \phi^{\rm NR}_{\rm metric}$, remains remarkably small ($\sim \pm 0.02$ radians) during the entire inspiral and plunge ($\omega_2 = 0.31$ being quite near the merger). By comparison, the root-sum of the various numerical errors on the phase (numerical truncation, outer boundary, extrapolation to infinity) is about 0.023 radians during the inspiral [29]. At the merger, and during the ringdown, $\Delta\phi$ takes somewhat larger values ($\sim \pm 0.1$ radians), but it oscillates around zero, so that, on average, it stays very well in phase with the NR waveform (as is clear on Fig. 9). By comparison, we note that [29] mentions that the phase error linked to the extrapolation to infinity doubles during ringdown. We then note that the total "two-sigma" NR error level estimated in [29] rises to 0.05 radians during ringdown, which is comparable to the EOB-NR phase disagreement. In addition, Ref. [40] compared the "improved" EOB waveform to accurate numerical relativity data (obtained by the Jena group [39]) on the coalescence of *unequal mass-ratio* black-hole binaries. Fig. 10 shows the result of the EOB/NR waveform comparison for a 2:1 mass ratio, corresponding to $\nu = 2/9$. When $a_5 = 0$, $a_6 = -20$ one finds $a_1 = -0.017017$ and $a_2 = 1.1906$. Again, the agreement is excellent, and within the numerical error bars.

Finally, Ref. [40] explored another aspect of the physical soundness of the EOB analytical formalism: the *triple* comparison between (i) the NR GW energy flux at infinity (which was computed in [28]); (ii) the corresponding analytically predicted GW energy flux at infinity (computed by summing $|\dot{h}_{\ell m}|^2$ over ℓ, m); and (iii) (minus) the *mechanical* energy loss of the system, as predicted by the general EOB

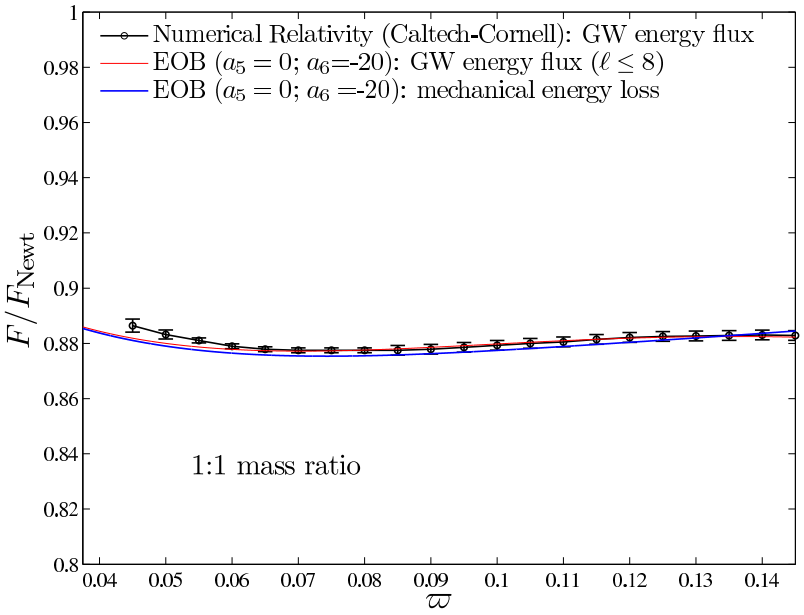

Fig. 11 The triple comparison between Numerical Relativity and EOB GW energy fluxes and the EOB mechanical energy loss.

formalism, i.e. the "work" done by the radiation reaction $\dot{E}_{\rm mechanical} = \Omega \mathscr{F}_\varphi$. This comparison is shown in Fig. 11, which should be compared to Fig. 9 of [28]. We kept here the same vertical scale as [28] which compared the NR flux to older versions of (resummed and non-resummed) analytical fluxes and needed such a $\pm 10\%$ vertical scale to accomodate all the models they considered. [The horizontal axis is the frequency ϖ of the differentiated metric waveform $\dot{h}_{22}$.] By contrast, we see again the striking closeness (at the $\sim 2 \times 10^{-3}$ level) between the EOB and NR GW fluxes. As both fluxes include higher multipoles than the $(2,2)$ one, this closeness is a further test of the agreement between the improved EOB formalism and NR results. [We think that the $\sim 2\sigma$ difference between the (coinciding) analytical curves and the NR one on the left of the Figure is due to uncertainties in the flux computation of [28], possibly related to the method used there of computing $\dot{h}$.] Note that the rather close agreement between the analytical energy flux and the mechanical energy loss during late inspiral is not required by physics (because of the well-known "Schott term" [104]), but is rather an indication that $\dot{h}_{\ell m}$ can be well approximated by $-im\Omega h_{\ell m}$

7 Conclusions

We have reviewed the basic elements of the Effective One Body (EOB) formalism. This formalism is still under development. The various existing versions of the EOB formalism have all shown their capability to reproduce within numerical errors the currently most accurate numerical relativity simulations of coalescing binary black holes. These versions differ in the number of free theoretical parameters. Recently a new "improved" version of the formalism has been defined which contains essentially only *two* free theoretical parameters.
Among the successes of the EOB formalism let us mention:

1. An analytical understanding of the non-adiabatic late-inspiral dynamics and of its "blurred" transition to a quasi-circular plunge;
2. The surprising possibility to analytically describe the merger of two black holes by a seemingly coarse approximation consisting of matching a continued inspiral to a ringdown signal;
3. The capability, after using suitable resummation methods, to reproduce with exquisite accuracy *both* the phase and the amplitude of the gravitational wave signal emitted during the entire coalescence process, from early-inspiral, to late-inspiral, plunge, merger and ringdown;
4. The gravitational wave energy flux predicted by the EOB formalism agrees, within numerical errors, with the most accurate numerical-relativity energy flux;
5. The ability to correctly estimate (within a 2% error) the final spin and mass of nonspinning coalescing black hole binaries [this issue has not been discussed in this review, but see Ref. [34]].

We anticipate that the EOB formalism will also be able to provide an accurate description of more complicated systems than the nonspinning BBH discussed in this review. On the one hand, we think that the recently improved EOB framework can be extended to the description of (nearly circularized) *spinning* black hole systems by suitably incorporating both the PN-expanded knowledge of spin effects [105, 106, 108] and their possible EOB resummation [4, 107]. On the other hand, the EOB formalism can also be extended to the description of binary neutron stars or mixed binary systems made of a black hole and a neutron star [109, 110]. An important input for this extension is the use of the relativistic tidal properties of neutron stars [111, 112, 113]

Finally, we think that the EOB formalism has opened the realistic possibility of constructing (with minimal computational resources) a very accurate, large bank of gravitational wave templates, thereby helping in both detecting and analyzing the signals emitted by inspiralling and coalescing binary black holes. Though we have had in mind in this review essentially ground-based detectors, we think that the EOB method can also be applied to space-based ones,i.e., to (possibly eccentric) large mass ratio systems.

Acknowledgments.

AN is grateful to Alessandro Spallicci, Bernard Whiting and all the organizers of the "Ecole thématique du CNRS sur la masse (origine, mouvement, mesure)".

Among the many colleagues whom we benefitted from, we would like to thank particularly Emanuele Berti, Bernd Brügmann, Alessandra Buonanno, Nils Dorband, Mark Hannam, Sascha Husa, Bala Iyer, Larry Kidder, Eric Poisson, Denis Pollney, Luciano Rezzolla, B.S. Sathyaprakash, Angelo Tartaglia and Loic Villain, for fruitful collaborations and discussions. We are also grateful to Marie-Claude Vergne for help with Fig. 1.

References

1. B. S. Sathyaprakash and B. F. Schutz, Physics, Astrophysics and Cosmology with Gravitational Waves, Living Rev. Rel. **12**, 2 (2009) [arXiv:0903.0338 [gr-qc]].
2. A. Buonanno and T. Damour, Effective one-body approach to general relativistic two-body dynamics, Phys. Rev. D **59**, 084006 (1999) [arXiv:gr-qc/9811091].
3. A. Buonanno and T. Damour, Transition from inspiral to plunge in binary black hole coalescences, Phys. Rev. D **62**, 064015 (2000) [arXiv:gr-qc/0001013].
4. T. Damour, Coalescence of two spinning black holes: An effective one-body approach, Phys. Rev. D **64**, 124013 (2001) [arXiv:gr-qc/0103018].
5. T. Damour, P. Jaranowski and G. Schäfer, On the determination of the last stable orbit for circular general relativistic binaries at the third post-Newtonian approximation, Phys. Rev. D **62**, 084011 (2000) [arXiv:gr-qc/0005034].
6. A. Buonanno, Y. Chen and T. Damour, Transition from inspiral to plunge in precessing binaries of spinning black holes, Phys. Rev. D **74**, 104005 (2006) [arXiv:gr-qc/0508067].
7. F. Pretorius, Evolution of Binary Black Hole Spacetimes, Phys. Rev. Lett. **95**, 121101 (2005) [arXiv:gr-qc/0507014].
8. F. Pretorius, Simulation of binary black hole spacetimes with a harmonic evolution scheme, Class. Quant. Grav. **23**, S529 (2006) [arXiv:gr-qc/0602115].
9. U. Sperhake, V. Cardoso, F. Pretorius, E. Berti and J. A. Gonzalez, The high-energy collision of two black holes, Phys. Rev. Lett. **101**, 161101 (2008) [arXiv:0806.1738 [gr-qc]].
10. M. Campanelli, C. O. Lousto, P. Marronetti and Y. Zlochower, Accurate Evolutions of Orbiting Black-Hole Binaries Without Excision, Phys. Rev. Lett. **96**, 111101 (2006) [arXiv:gr-qc/0511048].
11. M. Campanelli, C. O. Lousto and Y. Zlochower, Gravitational radiation from spinning-black-hole binaries: The orbital hang up, Phys. Rev. D **74**, 041501 (2006) [arXiv:gr-qc/0604012].
12. M. Campanelli, C. O. Lousto and Y. Zlochower, The last orbit of binary black holes, Phys. Rev. D **73**, 061501 (2006) [arXiv:gr-qc/0601091].
13. M. Campanelli, C. O. Lousto, Y. Zlochower and D. Merritt, Maximum gravitational recoil, Phys. Rev. Lett. **98**, 231102 (2007) [arXiv:gr-qc/0702133].
14. J. G. Baker, J. Centrella, D. I. Choi, M. Koppitz and J. van Meter, Gravitational wave extraction from an inspiraling configuration of merging black holes, Phys. Rev. Lett. **96**, 111102 (2006) [arXiv:gr-qc/0511103].
15. J. G. Baker, J. Centrella, D. I. Choi, M. Koppitz and J. van Meter, Binary black hole merger dynamics and waveforms, Phys. Rev. D **73**, 104002 (2006) [arXiv:gr-qc/0602026].
16. J. G. Baker, J. Centrella, D. I. Choi, M. Koppitz, J. R. van Meter and M. C. Miller, Getting a kick out of numerical relativity, Astrophys. J. **653**, L93 (2006) [arXiv:astro-ph/0603204].
17. J. G. Baker, M. Campanelli, F. Pretorius and Y. Zlochower, Comparisons of binary black hole merger waveforms, Class. Quant. Grav. **24**, S25 (2007) [arXiv:gr-qc/0701016].
18. J. A. Gonzalez, U. Sperhake, B. Bruegmann, M. Hannam and S. Husa, Total recoil: the maximum kick from nonspinning black-hole binary inspiral, Phys. Rev. Lett. **98**, 091101 (2007) [arXiv:gr-qc/0610154].
19. J. A. Gonzalez, M. D. Hannam, U. Sperhake, B. Bruegmann and S. Husa, Supermassive kicks for spinning black holes, Phys. Rev. Lett. **98**, 231101 (2007) [arXiv:gr-qc/0702052].
20. S. Husa, M. Hannam, J. A. Gonzalez, U. Sperhake and B. Bruegmann, Reducing eccentricity in black-hole binary evolutions with initial parameters from post-Newtonian inspiral, Phys. Rev. D **77**, 044037 (2008) [arXiv:0706.0904 [gr-qc]].
21. M. Koppitz, D. Pollney, C. Reisswig, L. Rezzolla, J. Thornburg, P. Diener and E. Schnetter, Getting a kick from equal-mass binary black hole mergers, Phys. Rev. Lett. **99**, 041102 (2007) [arXiv:gr-qc/0701163].
22. D. Pollney *et al.*, Recoil velocities from equal-mass binary black-hole mergers: a systematic investigation of spin-orbit aligned configurations, Phys. Rev. D **76**, 124002 (2007) [arXiv:0707.2559 [gr-qc]].

23. L. Rezzolla, E. N. Dorband, C. Reisswig, P. Diener, D. Pollney, E. Schnetter and B. Szilagyi, Spin Diagrams for Equal-Mass Black-Hole Binaries with Aligned Spins, Astrophysics **J679**, 1422 (2008) [arXiv:0708.3999 [gr-qc]].
24. L. Rezzolla, P. Diener, E. N. Dorband, D. Pollney, C. Reisswig, E. Schnetter and J. Seiler, The final spin from the coalescence of aligned-spin black-hole binaries, Astrophys. J. **674**, L29 (2008) [arXiv:0710.3345 [gr-qc]].
25. L. Rezzolla, E. Barausse, E. N. Dorband, D. Pollney, C. Reisswig, J. Seiler and S. Husa, On the final spin from the coalescence of two black holes, Phys. Rev. D **78**, 044002 (2008) [arXiv:0712.3541 [gr-qc]].
26. M. Boyle, L. Lindblom, H. Pfeiffer, M. Scheel and L. E. Kidder, Testing the Accuracy and Stability of Spectral Methods in Numerical Relativity, Phys. Rev. D **75**, 024006 (2007) [arXiv:gr-qc/0609047].
27. M. Boyle *et al.*, High-accuracy comparison of numerical relativity simulations with post-Newtonian expansions, Phys. Rev. D **76**, 124038 (2007) [arXiv:0710.0158 [gr-qc]].
28. M. Boyle, A. Buonanno, L. E. Kidder, A. H. Mroue, Y. Pan, H. P. Pfeiffer and M. A. Scheel, High-accuracy numerical simulation of black-hole binaries: Computation of the gravitational-wave energy flux and comparisons with post-Newtonian approximants, Phys. Rev. D **78**, 104020 (2008) [arXiv:0804.4184 [gr-qc]].
29. M. A. Scheel, M. Boyle, T. Chu, L. E. Kidder, K. D. Matthews and H. P. Pfeiffer, High-accuracy waveforms for binary black hole inspiral, merger, and ringdown, Phys. Rev. D **79**, 024003 (2009) [arXiv:0810.1767 [gr-qc]].
30. F. Pretorius, Binary Black Hole Coalescence . The final version of this Lecture Note will appear in the book: *Relativistic Objects in Compact Binaries: From Birth to Coalescense*, M. Colpi et al. Eds.,Springer Verlag, Canopus Publishing Limited, arXiv:0710.1338 [gr-qc]
31. A. Buonanno, G. B. Cook and F. Pretorius, Inspiral, merger and ring-down of equal-mass black-hole binaries, Phys. Rev. D **75**, 124018 (2007) [arXiv:gr-qc/0610122].
32. Y. Pan *et al.*, A data-analysis driven comparison of analytic and numerical coalescing binary waveforms: Nonspinning case, Phys. Rev. D **77**, 024014 (2008) [arXiv:0704.1964 [gr-qc]].
33. A. Buonanno, Y. Pan, J. G. Baker, J. Centrella, B. J. Kelly, S. T. McWilliams and J. R. van Meter, Toward faithful templates for non-spinning binary black holes using the effective-one-body approach, Phys. Rev. D **76**, 104049 (2007) [arXiv:0706.3732 [gr-qc]].
34. T. Damour and A. Nagar, Final spin of a coalescing black-hole binary: An effective-one-body approach, Phys. Rev. D **76**, 044003 (2007) [arXiv:0704.3550 [gr-qc]].
35. A. Nagar, T. Damour and A. Tartaglia, Binary black hole merger in the extreme mass ratio limit, Class. Quant. Grav. **24**, S109 (2007) [arXiv:gr-qc/0612096].
36. T. Damour and A. Nagar, Faithful Effective-One-Body waveforms of small-mass-ratio coalescing black-hole binaries, Phys. Rev. D **76**, 064028 (2007) [arXiv:0705.2519 [gr-qc]].
37. T. Damour and A. Nagar, Comparing Effective-One-Body gravitational waveforms to accurate numerical data, Phys. Rev. D **77**, 024043 (2008) [arXiv:0711.2628 [gr-qc]].
38. T. Damour, A. Nagar, E. N. Dorband, D. Pollney and L. Rezzolla, Faithful Effective-One-Body waveforms of equal-mass coalescing black-hole binaries, Phys. Rev. D **77**, 084017 (2008) [arXiv:0712.3003 [gr-qc]].
39. T. Damour, A. Nagar, M. Hannam, S. Husa and B. Bruegmann, Accurate Effective-One-Body waveforms of inspiralling and coalescing black-hole binaries, Phys. Rev. D **78**, 044039 (2008) [arXiv:0803.3162 [gr-qc]].
40. T. Damour and A. Nagar, An improved analytical description of inspiralling and coalescing black-hole binaries, arXiv:0902.0136 [gr-qc].
41. A. Buonanno, Y. Pan, H. P. Pfeiffer, M. A. Scheel, L. T. Buchman and L. E. Kidder, Effective-one-body waveforms calibrated to numerical relativity simulations: coalescence of non-spinning, equal-mass black holes, arXiv:0902.0790 [gr-qc].
42. J. G. Baker, J. R. van Meter, S. T. McWilliams, J. Centrella and B. J. Kelly, Consistency of post-Newtonian waveforms with numerical relativity, Phys. Rev. Lett. **99**, 181101 (2007) [arXiv:gr-qc/0612024

43. M. Hannam, S. Husa, U. Sperhake, B. Bruegmann and J. A. Gonzalez, Where post-Newtonian and numerical-relativity waveforms meet, Phys. Rev. D **77**, 044020 (2008) [arXiv:0706.1305 [gr-qc]].
44. P. Ajith *et al.*, Phenomenological template family for black-hole coalescence waveforms, Class. Quant. Grav. **24**, S689 (2007) [arXiv:0704.3764 [gr-qc]].
45. P. Ajith *et al.*, A template bank for gravitational waveforms from coalescing binary black holes: I. non-spinning binaries, Phys. Rev. D **77**, 104017 (2008) [arXiv:0710.2335 [gr-qc]].
46. A. Gopakumar, M. Hannam, S. Husa and B. Bruegmann, Comparison between numerical relativity and a new class of post-Newtonian gravitational-wave phase evolutions: the non-spinning equal-mass case, Phys. Rev. D **78**, 064026 (2008) [arXiv:0712.3737 [gr-qc]].
47. M. Hannam, S. Husa, B. Bruegmann and A. Gopakumar, Comparison between numerical-relativity and post-Newtonian waveforms from spinning binaries: the orbital hang-up case, Phys. Rev. D **78**, 104007 (2008) [arXiv:0712.3787 [gr-qc]].
48. E. Brezin, C. Itzykson and J. Zinn-Justin, Relativistic balmer formula including recoil effects, Phys. Rev. D **1**, 2349 (1970).
49. T. Damour, B. R. Iyer and B. S. Sathyaprakash, Improved filters for gravitational waves from inspiralling compact binaries, Phys. Rev. D **57**, 885 (1998) [arXiv:gr-qc/9708034].
50. T. Damour, B. R. Iyer and A. Nagar, Improved resummation of post-Newtonian multipolar waveforms from circularized compact binaries, arXiv:0811.2069 [gr-qc].
51. M. Davis, R. Ruffini and J. Tiomno, Pulses of gravitational radiation of a particle falling radially into a Schwarzschild black hole, Phys. Rev. D **5**, 2932 (1972).
52. R. H. Price and J. Pullin, Colliding black holes: The Close limit, Phys. Rev. Lett. **72**, 3297 (1994) [arXiv:gr-qc/9402039].
53. T. Damour and N. Deruelle, Radiation Reaction And Angular Momentum Loss In Small Angle Gravitational Scattering, Phys. Lett. A **87**, 81 (1981).
54. T. Damour, Gravitational Radiation And The Motion Of Compact Bodies,, in *Gravitational Radiation*, N. Deruelle and T. Piran Eds, 1983, North Holland, Amsterdam, p 59-144.
55. G. Schäfer, The gravitational quadrupole radiation reaction force and the canonical formalism of ADM, Annals Phys. **161**, 81 (1985).
56. S. M. Kopejkin: Astron. Zh. **62**, 889 (1985).
57. P. Jaranowski and G. Schäfer, 3rd post-Newtonian higher order Hamilton dynamics for two-body point-mass systems, Phys. Rev. D **57**, 7274 (1998) [Erratum-ibid. D **63**, 029902 (2001)] [arXiv:gr-qc/9712075].
58. L. Blanchet and G. Faye, General relativistic dynamics of compact binaries at the third post-Newtonian order, Phys. Rev. D **63**, 062005 (2001) [arXiv:gr-qc/0007051].
59. T. Damour, P. Jaranowski and G. Schäfer, Dimensional regularization of the gravitational interaction of point masses, Phys. Lett. B **513**, 147 (2001) [arXiv:gr-qc/0105038].
60. L. Blanchet, T. Damour and G. Esposito-Farese, Dimensional regularization of the third post-Newtonian dynamics of point particles in harmonic coordinates," Phys. Rev. D **69**, 124007 (2004) [arXiv:gr-qc/0311052].
61. Y. Itoh and T. Futamase, New derivation of a third post-Newtonian equation of motion for relativistic compact binaries without ambiguity, Phys. Rev. D **68**, 121501 (2003) [arXiv:gr-qc/0310028].
62. M. E. Pati and C. M. Will, Post-Newtonian gravitational radiation and equations of motion via direct integration of the relaxed Einstein equations. II: Two-body equations of motion to second post-Newtonian order, and radiation-reaction to 3.5 post-Newton, Phys. Rev. D **65**, 104008 (2002) [arXiv:gr-qc/0201001].
63. C. Konigsdorffer, G. Faye and G. Schäfer, The binary black-hole dynamics at the third-and-a-half post-Newtonian order in the ADM-formalism," Phys. Rev. D **68**, 044004 (2003) [arXiv:gr-qc/0305048].
64. S. Nissanke and L. Blanchet, Gravitational radiation reaction in the equations of motion of compact binaries to 3.5 post-Newtonian order," Class. Quant. Grav. **22**, 1007 (2005) [arXiv:gr-qc/0412018].
65. L. Blanchet and T. Damour, Radiative gravitational fields in general relativity I. General structure of the field outside the source, Phil. Trans. Roy. Soc. Lond. A **320**, 379 (1986).

66. L. Blanchet and T. Damour, Postnewtonian generation of gravitational waves, Annales Poincare Phys. Theor. **50** 377, (1989).
67. T. Damour and B. R. Iyer, Multipole analysis for electromagnetism and linearized gravity with irreducible cartesian tensors, Phys. Rev. D **43**, 3259 (1991).
68. T. Damour and B. R. Iyer, PostNewtonian generation of gravitational waves. 2. The Spin moments, Annales Poincare Phys. Theor. **54**, 115 (1991).
69. L. Blanchet and T. Damour, Hereditary Effects In Gravitational Radiation, Phys. Rev. D **46**, 4304 (1992).
70. L. Blanchet, Second Postnewtonian Generation Of Gravitational Radiation, Phys. Rev. D **51**, 2559 (1995) [arXiv:gr-qc/9501030].
71. L. Blanchet, Gravitational-wave tails of tails, Class. Quant. Grav. **15**, 113 (1998) [Erratum-ibid. **22**, 3381 (2005)] [arXiv:gr-qc/9710038].
72. C. M. Will and A. G. Wiseman, Gravitational radiation from compact binary systems: gravitational waveforms and energy loss to second post-Newtonian order, Phys. Rev. D **54**, 4813 (1996) [arXiv:gr-qc/9608012].
73. C. M. Will, Generation of post-Newtonian gravitational radiation via direct integration of the relaxed Einstein equations, Prog. Theor. Phys. Suppl. **136**, 158 (1999) [arXiv:gr-qc/9910057].
74. M. E. Pati and C. M. Will, Post-Newtonian gravitational radiation and equations of motion via direct integration of the relaxed Einstein equations. I: Foundations, Phys. Rev. D **62**, 124015 (2000) [arXiv:gr-qc/0007087].
75. L. Blanchet, T. Damour, B. R. Iyer, C. M. Will and A. G. Wiseman, Gravitational Radiation Damping Of Compact Binary Systems To Second Postnewtonian Order, Phys. Rev. Lett. **74**, 3515 (1995) [arXiv:gr-qc/9501027].
76. L. Blanchet, T. Damour and B. R. Iyer, Gravitational Waves From Inspiralling Compact Binaries: Energy Loss And Wave Form To Second Postnewtonian Order, Phys. Rev. D **51**, 5360 (1995) [Erratum-ibid. D **54**, 1860 (1996)] [arXiv:gr-qc/9501029].
77. L. Blanchet, B. R. Iyer and B. Joguet, Gravitational waves from inspiralling compact binaries: Energy flux to third post-Newtonian order, Phys. Rev. D **65**, 064005 (2002) [Erratum-ibid. D **71**, 129903 (2005)] [arXiv:gr-qc/0105098].
78. L. Blanchet and B. R. Iyer, Hadamard regularization of the third post-Newtonian gravitational wave generation of two point masses, Phys. Rev. D **71**, 024004 (2005) [arXiv:gr-qc/0409094].
79. A. G. Wiseman, Coalescing Binary Systems Of Compact Objects To (Post)Newtonian5/2 Order.4v: The Gravitational Wave Tail, Phys. Rev. D **48**, 4757 (1993).
80. L. Blanchet and G. Schä fer, Gravitational wave tails and binary star systems, Class. Quant. Grav. **10**, 2699 (1993).
81. L. Blanchet, T. Damour, G. Esposito-Farese and B. R. Iyer, Gravitational radiation from inspiralling compact binaries completed at the third post-Newtonian order, Phys. Rev. Lett. **93**, 091101 (2004) [arXiv:gr-qc/0406012].
82. L. Blanchet, T. Damour, G. Esposito-Farese and B. R. Iyer, Dimensional regularization of the third post-Newtonian gravitational wave generation from two point masses, Phys. Rev. D **71**, 124004 (2005) [arXiv:gr-qc/0503044].
83. L. Blanchet, Gravitational radiation from post-Newtonian sources and inspiralling compact binaries, Living Rev. Rel. **5**, 3 (2002) [arXiv:gr-qc/0202016].
84. T. Damour, B. R. Iyer and B. S. Sathyaprakash, A comparison of search templates for gravitational waves from binary inspiral, Phys. Rev. D **63**, 044023 (2001) [Erratum-ibid. D **72**, 029902 (2005)] [arXiv:gr-qc/0010009].
85. L. Blanchet, G. Faye, B. R. Iyer and B. Joguet, Gravitational-wave inspiral of compact binary systems to 7/2 post-Newtonian order, Phys. Rev. D **65**, 061501 (2002) [Erratum-ibid. D **71**, 129902 (2005)] [arXiv:gr-qc/0105099].
86. J. G. Baker, S. T. McWilliams, J. R. van Meter, J. Centrella, D. I. Choi, B. J. Kelly and M. Koppitz, Binary black hole late inspiral: Simulations for gravitational wave observations, Phys. Rev. D **75**, 124024 (2007) [arXiv:gr-qc/0612117].

87. T. Damour and G. Schäfer, Higher order relativistic periastron advances and binary pulsars, Nuovo Cim. B **101**, 127 (1988).
88. T. Damour, B. R. Iyer, P. Jaranowski and B. S. Sathyaprakash, Gravitational waves from black hole binary inspiral and merger: The span of third post-Newtonian effective-one-body templates, Phys. Rev. D **67**, 064028 (2003) [arXiv:gr-qc/0211041].
89. T. Damour, E. Gourgoulhon and P. Grandclement, Circular orbits of corotating binary black holes: Comparison between analytical and numerical results, Phys. Rev. D **66**, 024007 (2002) [arXiv:gr-qc/0204011].
90. T. Damour and A. Gopakumar, Gravitational recoil during binary black hole coalescence using the effective one body approach, Phys. Rev. D **73**, 124006 (2006) [arXiv:gr-qc/0602117].
91. H. Tagoshi and M. Sasaki, PostNewtonian expansion of gravitational waves from a particle in circular orbit around a Schwarzschild black hole, Prog. Theor. Phys. **92**, 745 (1994) [arXiv:gr-qc/9405062].
92. C. Cutler, E. Poisson, G. J. Sussman and L. S. Finn, Gravitational radiation from a particle in circular orbit around a black hole. 2: Numerical results for the nonrotating case, Phys. Rev. D **47**, 1511 (1993).
93. N. Yunes and E. Berti, Accuracy of the Post-Newtonian Approximation: Optimal Asymptotic Expansion for Quasi-Circular, Extreme-Mass Ratio Inspirals, Phys. Rev. D **77**, 124006 (2008) [arXiv:0803.1853 [gr-qc]].
94. E. Poisson, Gravitational radiation from a particle in circular orbit around a black hole. 6. Accuracy of the postNewtonian expansion, Phys. Rev. D **52**, 5719 (1995) [Addendum-ibid. D **55**, 7980 (1997)] [arXiv:gr-qc/9505030].
95. H. Tagoshi and M. Sasaki, PostNewtonian expansion of gravitational waves from a particle in circular orbit around a Schwarzschild black hole, Prog. Theor. Phys. **92**, 745 (1994) [arXiv:gr-qc/9405062].
96. T. Tanaka, H. Tagoshi and M. Sasaki, Gravitational waves by a particle in circular orbits around a Schwarzschild black hole: 5.5 post-Newtonian formula, Prog. Theor. Phys. **96**, 1087 (1996) [arXiv:gr-qc/9701050].
97. T. Damour, B. R. Iyer, P. Jaranowski and B. S. Sathyaprakash, Gravitational waves from black hole binary inspiral and merger: The span of third post-Newtonian effective-one-body templates, Phys. Rev. D **67**, 064028 (2003) [arXiv:gr-qc/0211041].
98. T. Tanaka, H. Tagoshi and M. Sasaki, Prog. Theor. Phys. **96** 1087 (1996), [arXiv:gr-qc/9701050v1].
99. L. E. Kidder, Using Full Information When Computing Modes of Post-Newtonian Waveforms From Inspiralling Compact Binaries in Circular Orbit, Phys. Rev. D **77**, 044016 (2008) [arXiv:0710.0614 [gr-qc]].
100. E. Berti, V. Cardoso, J. A. Gonzalez, U. Sperhake, M. Hannam, S. Husa and B. Bruegmann, Inspiral, merger and ringdown of unequal mass black hole binaries: A multipolar analysis, Phys. Rev. D **76**, 064034 (2007) [arXiv:gr-qc/0703053].
101. L. Blanchet, G. Faye, B. R. Iyer and S. Sinha, The third post-Newtonian gravitational wave polarisations and associated spherical harmonic modes for inspiralling compact binaries in quasi-circular orbits, arXiv:0802.1249 [gr-qc].
102. L. Blanchet, Quadrupole-quadrupole gravitational waves, Class. Quant. Grav. **15**, 89 (1998) [arXiv:gr-qc/9710037].
103. L. Blanchet, Gravitational-wave tails of tails, Class. Quant. Grav. **15**, 113 (1998) [Erratum-ibid. **22**, 3381 (2005)] [arXiv:gr-qc/9710038].
104. G. A. Schott, Phil. Mag. **29**, 49, (1915).
105. G. Faye, L. Blanchet and A. Buonanno, Higher-order spin effects in the dynamics of compact binaries. I: Equations of motion, Phys. Rev. D **74**, 104033 (2006) [arXiv:gr-qc/0605139].
106. T. Damour, P. Jaranowski and G. Schäfer, Hamiltonian of two spinning compact bodies with next-to-leading order gravitational spin-orbit coupling, Phys. Rev. D **77**, 064032 (2008) [arXiv:0711.1048 [gr-qc]].
107. T. Damour, P. Jaranowski and G. Schäfer, Effective one body approach to the dynamics of two spinning black holes with next-to-leading order spin-orbit coupling, Phys. Rev. D **78**, 024009 (2008) [arXiv:0803.0915 [gr-qc]].

108. K. G. Arun, A. Buonanno, G. Faye and E. Ochsner, Higher-order spin effects in the amplitude and phase of gravitational waveforms emitted by inspiraling compact binaries: Ready-to-use gravitational waveforms, arXiv:0810.5336 [gr-qc].
109. T. Damour and A. Nagar, in preparation.
110. T. Damour, A. Nagar and L. Villain, in preparation.
111. T. Hinderer, Tidal Love numbers of neutron stars, Astrophys. J. **677**, 1216 (2008) [arXiv:0711.2420 [astro-ph]].
112. T. Damour and A. Nagar, Relativistic tidal properties of neutron stars, arXiv:0906.0096 [gr-qc].
113. T. Binnington and E. Poisson, Relativistic theory of tidal Love numbers, arXiv:0906.1366 [gr-qc].